



Precise tool manipulation and positioning of
a soft sensorised anthropomorphic hand through
feedback control and machine learning

Author: **Louis Relandreau**

M.Eng. Thesis, ljgmr2@cam.ac.uk, Girton College

Supervisor: **Prof. Fumiya Iida**

Professor of Robotics, Principal Investigator of the Bio-Inspired Robotics Lab

Co-Supervisor: **Kieran Gilday**

PhD Student in the Bio-Inspired Robotics Lab

I hereby declare that, except where specifically indicated,
the work submitted herein is my own original work.

Signed:

A handwritten signature in black ink, appearing to read "Louis Relandreau".

Date: 1st June 2022

Precise tool manipulation and positioning of a soft sensorised anthropomorphic hand through feedback control and machine learning

Fourth-Year Undergraduate Project (F-FI224-1) in Division F, 2021/2022

Bio-Inspired Robotics Laboratory, Department of Engineering, University of Cambridge

Louis Relandeau (ljgmr2), Girton College

Supervised by Dr. Fumiya Iida and Kieran Gilday

Technical Abstract

Current robotic implementations are struggling to move away from the highly controllable industrial settings towards the more chaotic and unpredictable human environments. As society evolves, there seems to be an increased need for such robots which can achieve a range of different tasks. This is true in many fields including healthcare, agriculture, rescue and personal service robots. When comparing human capabilities to those of existing robots, there are many disparities. The capacity to adapt to new situations, agility, dexterity, and tactile sensing, are all superior for human beings. While robots excel in vision and auditory sensing, their tactile sensing is often reduced, limiting the scope of interactions with their environment. On the other hand, the human hand contains an extreme receptor density, particularly in fingertips, with over 17,000 tactile mechanoreceptors enabling fast feedback of contact forces, temperature and textures. By making robots more human-like, their capabilities to navigate and interact with human environments improves. This makes robotic manipulation an ongoing research area with increasingly diverse applications.

The goal of this project is to improve robotic manipulation capabilities by presenting a novel tactile sensing technology relying on barometric sensing. The proposed solution is a soft silicone skin containing air chambers which change in volume when the skin deforms under contact. The chambers are connected to barometric sensors which continuously measure their internal pressure and provide feedback to the controller. This skin is molded over a 3D printed anthropomorphic skeleton-like hand resulting in a low-cost and highly customisable solution.

Previous research has shown the potential of soft materials, often inspired from biological systems, for improved performance in noisy environments. Embedded compliancy enables a shift of complexity from the controller to the non-linear dynamics of the soft system. However, the issue with soft materials is the difficulty to integrate them with traditional hard sensors. Such sensors constrain surface materials resulting in poor soft properties (e.g. low friction and low deformation) and their use is often limited by interfaces issues with soft components. Although many tactile sensing implementation exist, no solution enables the high design freedom allowed by the proposed approach while maintaining fine sensing and good material properties.

Tasks requiring tactile feedback in robotic manipulation are hugely diverse so choices were made to limit the scope of this project. for this reason, this thesis focus on the problems of data interpretation for tool use. The use of tools demonstrates in-hand manipulation, exploration and dexterity for anthropomorphic hands. Moreover, for a robot to fully integrate in human environments it must be able to use tools designed for humans. Taking a specific example: using a screwdriver to screw a screw, it can be decomposed into a set of different problems. Understanding 3-axis contact modelling (i.e. how the sensors in the skin respond to contacts) is the first requirement. A solution to this problem is presented through the use of machine learning for data interpretation; the orientation of a contact can be predicted solely from tactile data. Results are presented for two topologies of neural networks. The second step in using a tool is remote sensing for exploration and feature detection. In the case of using a screwdriver, this would be finding the screw head and placing the screwdriver appropriately in the screw drive. To mimic this scenario, the classic robotic peg-in-hole assembly was implemented using a chopstick pinched between two fingers. This system is successfully able to search and detect a small (5mm) hole in a flat table before inserting the chopstick in it.

Such problems can be resolved thanks to careful sensor placement in the soft skin, allowed by a very configurable design. Sensors can be placed in closed proximity (2-4mm) to mimic the dense tactile inputs in human skin. The sensors characteristics also allow for very precise sensing. By mounting the hand on a UR5 robotic arm for repeatable testing, the sensors were characterised as being able to detect forces ranging from 23mN to 5700mN and having a bandwidth of 20Hz. These parameters exceed the typical requirements for exploration, grasping and dexterous manipulation.

In conclusion, this thesis reports the potential of a novel soft sensing approach through characterisation data and a remote sensing application using a tool. This opens directions for further research in the hope of enabling such technology to become readily accessible for any robotic system concerned with manipulation and tactile sensing.

Contents

1	Introduction	1
1.1	Motivation	1
1.2	Contributions	2
1.3	Thesis Structure	2
2	Background	4
2.1	Robotic Hands	4
2.2	Sensors	6
2.3	Materials	7
2.4	Modelling and Data Interpretation	8
2.5	Control	9
2.6	Previous Work	9
3	Experimental Apparatus and Methods	11
3.1	Sensorised Skin Manufacturing	11
3.2	System Framework	13
3.3	Sensor Characterisation	15
3.4	Tool Manipulation and Sensing Experiments	16
3.4.1	Picking	16
3.4.2	Orientation Prediction with Neural Networks	17
3.4.3	Hole Detection and Peg-in-hole Problem	20
4	Results and Discussion	23
4.1	Sensor Characterisation	23
4.2	Tool Manipulation and Sensing Experiments	27
4.2.1	Picking	27
4.2.2	Orientation Prediction with Neural Networks	28
4.2.3	Hole Detection and Peg-in-hole Problem	30
4.3	Noise analysis	32
5	Conclusions	36
5.1	Main Findings	36
5.2	Limitations	37

5.3 Future work	38
Bibliography	39
6 Appendices	43
Risk Assessment Retrospective	43
Acknowledgments	43
Additional Resources	44

List of Figures

2.1 Anthropomorphic hand implementations, from left to right: TUAT hand [14], Xu’s highly anthropomorphic hand [11], and BCL-26 soft robotic hand [5].	6
2.2 Anthropomorphic skeleton from [42] and [54] for hand used in this project shown to achieve example grasp types from the GRASP taxonomy (Image from [54]).	10
3.1 Sensorised hand and mold design. Exploded view shows the skin model (1st from top) and skeleton mold (2nd from top) used to make the hand skin mold (bottom). The created mold is then modified to add the custom air chambers in the desired locations (3rd from top). The section analysis shows a pair of air chambers in the middle fingertip.	12
3.2 Sensorised hand fabrication. (a) Printed inner and chamber molds. (b) Fully assembled mold. (c) Tendon-driven, anatomical hand with thumb, index and middle finger. (d) Skin cast with Ecoflex 00-30 silicone. (e) Hand with 32 sensors, 10 in each finger (6 in fingertips), 2 in the palm.	12
3.3 Annotated hand with sensorised skin and servomotor actuation mechanism.	13
3.4 Overall framework diagram presenting experimental setup and connections between modules.	14
3.5 Flowchart of software implementation for open-loop controller for data collection experiments.	14
3.6 (a) Sample skin dimensions: distance between air chamber and surface of the skin (depth) and total skin thickness. (b) Labelled sensor samples. Each column is placed the same way in the skin, each row is a different receptor design, top to bottom: long elbow, short elbow, spherical. (c) Experimental setup for measuring sensor response under controlled loads.	15
3.7 (a) Air chamber locations in skin for 16 sensors used. (b) Experimental setup used for pinching data collection. Example of picking with a chopstick.	17

3.8	Experimental setup for data collection of wrist orientation data and tactile fingertip data.	18
3.9	Comparaison of ANNs and RNNs (LSTM) topologies.	19
3.10	ANN and LSTM network architectures (layer types and sizes) used for hand orientation prediction from fingertip sensor data.	20
3.11	Model of fingertip sensor compression when the pinched chopstick is rotated by a certain angle $\Delta\alpha$. The compliancy of the soft skin and skeleton provides a restoring moment M. The right hand side sketch shows the model used to derive (3.1) for the hole detection problem (d is the diameter of the hole detected).	21
3.12	Experimental setup for hole detection on a flat surface using a chopstick as a tool for remote sensing. Chopstick is dragged across laser-cut board with varying size holes.	22
4.1	Results from skin sample tests, sensor number corresponds to Figure 3.6b. Measured sensor pressure with varying indent tool (4, 8, 15mm) and force (0.25, 0.49, 0.98N).	23
4.2	Results from skin sample tests, sensor number corresponds to Figure 3.6b. Measured sensor pressure against distance from sensor centre for a constant force (0.98N) and indent tool (4mm).	24
4.3	(a) Short term step response of a single sensor as hand opens from pinching grasp. (b) Long-term step response of a single sensor pressed against surface.	25
4.4	Repeatability of 500 successive contact between index fingertip and surface for a single sensor.	25
4.5	Comparison of results between sensor data when pinching with and without chopstick in between index and thumb.	27
4.6	Comparison of hand orientations between real data and predictions from the ANN and LSTM neural networks.	29
4.7	Data collection for minimum angle detectable. Minimum detectable displacement $d = 4\text{mm}$ ($\Delta\alpha = 1.3^\circ$).	31
4.8	Experimental and theoretical (from (3.1)) results showing the smallest hole diameter detected for varying chopstick angle α , with experimental setup shown (left).	31
4.9	Example of raw and smoothed low-pass filtered (0.2Hz) signals for minimum detectable angle, data from Figure 4.7. Raw sensor data is dimensionless.	32
4.10	High-pass filter (0.2Hz) applied to raw signal of Figure 4.9.	33
4.11	Noise analysis using sum of Gaussian functions, noise value probabilities from signal shown in Figure 4.10.	34

List of Tables

4.1	Minimum and maximum forces observable with a voltmeter and the <i>4mm</i> impressioning tool for sensors 0 and 11.	24
4.2	Sensor characterisation results summary and comparison with other tactile sensors.	26
4.3	Summary of neural network topologies, training data, hyperparameters and output results for ANN and LSTM.	29
4.4	Sensor noise sources and mitigating solutions.	35

Chapter 1

Introduction

1.1 Motivation

Despite decades of development, dexterous manipulation with robotic hands is still an unsolved problem [1], [2]. The recent trend in soft robotics has led to many developments in soft robotic manipulation, with improved robustness in uncertain environments, passive adaptation, emerging behaviours to simplify control for grasping or basic manipulations [3], [4], [5], and increased versatility through environmental constraints exploitation [6]. The next step in improving dexterous manipulation is to integrate sensing with these soft technologies [7]. Sensors are a necessary features of all animals and robots, allowing them to understand the environment in which they are located, move appropriately and interact with surrounding objects.

Currently, robots lack the adaptability humans have when asked to perform a diverse range of tasks. This is arguably because of the fine sensing and feedback human brains get from millions of nerve endings in the skin. Even with improvements in materials and manufacturing processes [8], integration of tactile sensors has been limited in soft hands. This is due to the complex design constraints of soft systems (e.g. skin-like components) which must retain a certain compliancy or physical properties. The integration of hard electronic components with soft materials can lead to issues at the junction between the two materials, complex non-linear data affected by the dynamic properties of the soft material and reduced performance from the soft materials. There are many ways to implement tactile sensing but there is a lack of high resolution soft sensing implementations and sensing technologies that can adapt to different hand morphologies and manufacturing processes, as indicated in this review [9].

1.2 Contributions

This project advances the research in soft tactile feedback, providing a novel type of soft sensorised skin. The primary use case of the soft sensorised material developed for this project is as a tactile skin for anthropomorphic hands. Its soft properties make it similar to human skin and highly desirable for dexterous manipulation tasks in all field of robotics. Skin has the particularity of being very compliant and having a very high friction coefficient, especially on the hands (0.62 ± 0.22) [10]. Silicone has the highest coefficient of friction measured in the aforementioned paper, almost as good as human skin (0.61 ± 0.21). By using this material to manufacture the robotic skin, such desirable properties are maximised, enabling picking with reduced normal force.

Detailed characterisation data, methodology used to collect said data, and environment interaction data from the sensors is shared to assess the performance of this soft skin. The sensors are shown to achieve very good performance, comparable to commercial solutions when it comes to sensitivity, force range, bandwidth and resolution.

By using simplified modelling, data interpretation through neural networks, and feedback control, the robotic hand is able to solve a range of manipulation problems in a noisy environment. This includes predicting the relative orientation of a surface with respect to the fingertip of the hand as well as detecting holes in a flat surface through tool-enabled remote sensing. By modelling the interaction between the tool and the environment, it is possible to predict what size hole the robot is able to detect depending on the sensors' placements and experimental setup. Non-linear behaviours of the soft components remain unaffected by the embedded sensing and can be utilised to improve the success rate of the tasks.

Using 3D printing and resin casting methods, the soft sensing skin can be easily designed and cheaply manufactured. Moreover, this is an approach to sensing which is extremely configurable; the air chambers and sensors can be rearranged in many different configurations, relocated in different areas of the skin depending on the use case and design constraints. This makes it an enviable solution for many different morphologies of robotic hands, grippers and any surface which may require tactile feedback or contact detection. Such applications are omnipresent in the fields of human-robot interaction, haptics and autonomous robotics.

1.3 Thesis Structure

Chapter 2 focuses on the background research that was done for this project. This extensive literature review is key to understanding the context of this project, existing technologies and how the project fits into modern research. It includes an overview of existing tactile sensors and their integration with anthropomorphic hands and grippers

for manipulation tasks. Details on how data interpretation and control are achieved is then investigated, along with existing modelling strategies. The work previously done with the hardware utilised for this project is described to introduce the anthropomorphic hand and soft skin developed by Kieran Gilday. Chapter 3 describes the theoretical models and experimental methods used throughout the characterisation of the sensors and the manipulation experiments. This also includes the experimental apparatus and framework developed for control and data collection. Chapter 4 presents the results obtained from the aforementioned experiments along with analysis and discussions regarding their implications and limitations, covering both sensor characterisation and data interpretation experiments. Finally, the last chapter summarises the main findings of this project, current limitations and suggested future work.

Chapter 2

Background

2.1 Robotic Hands

With the increasing use of robots in human environments, in opposition to industrial settings, the need for high-performance anthropomorphic grippers is constantly increasing. This review therefore starts with an examination of existing robotic hands, allowing an understanding of the current limitations of robotic hands and emphasizing the need for precise sensing.

There have been many robotic hand designs over the past decades and this review by no means explores every single existing solution but attempts to cover the spectrum of relevant implementations. The first hand considered is the Highly Biomimetic Anthropomorphic Robotic Hand by Zhe Xu and Emanuel Todorov [11]. This anthropomorphic robotic hand is very close to the human hand in morphology, actuation and range of motion. It relies on a tendon actuated system with crocheted ligaments and extensor hood to perform a range of teleoperated grasps and in-hand manipulations. The design is complex but shows the potential of anthropomorphic approaches. Millions of years of evolution have fashioned the human hand to be an extremely dexterous and effective tool so taking inspiration from it is likely to produce promising results. A similar approach with a tendon driven bone structure-like hand is the ACT hand [12] which also shows great dexterity. Both these implementations focus on replicating anatomical, skeleton and motion characteristics of a hand rather than the sensing. Although this is clearly the first step in improving dexterous manipulation, this research shows that without sensing, the hand is limited to open-loop control of pre-programmed actions or visual teleoperation. The authors suggest the use of a previously developed force sensor that could replace the fingertip of their hand [13]. However, this heavily contrasts with the bio-inspiration and anthropomorphic objectives of the design. The proposed solution cannot be extend to cover the whole surface of the fingers and palm and provides only 3-axis force values for the last phalanx of the fingers. Human hands include approximately 17,000 nerve end-

ings which continuously detect and send pressure, vibration and temperature information to the brain. It is therefore clear that sensors for robotic hands should most likely be multi-modal and present in high density.

Another common approach to hand designs is to use rigid links for actuation as shown by the TUAT/Karlsruhe Humanoid Hand [14]. This is a little further away from the human morphology, it is less compliant but exhibits better controllability. This is the only design which claims to be able to use chopsticks although an auxiliary device was required, as shown in Figure 2.1. The authors highlight the dexterity required to achieve a range of grasps and the clever use of urethane gel patches to act as a skin, improving friction. Thanks to its structure, the hand can adjust grasp shape and force automatically. The authors argue that this removes need for tactile sensing and feedback control. Indeed, this works very well when controlling the grasping force of the robotic hand, which can be adjusted through careful actuation. If this hand was to be used as a prosthetic by a human user or on a humanoid robot, it could only be operated with an additional sensing mechanism to see what they are doing (i.e. a vision system). However, this is impractical and limited for tasks involving fine manipulation or high levels of occlusion. The use of urethane gel to create a skin-like surface on the hand is shown to greatly improve the grasping stability of many grips. This idea of covering a semi-rigid structure with a soft one to increase the overall compliancy mimics human anatomy, revealing very promising results.

There are other very dexterous hands such as the very recent BCL-26 [5] which is entirely soft and relies pneumatic chambers to control joint angles. The passive compliance embedded in the design allows for many complex grasps and tasks such as in-hand manipulation and writing. This hand shows promise considering that it is entirely soft and could include embedded sensors during the casting process. The manufacturing process is also greatly simplified but the modelling and control of interactions with objects is much harder to simulate. Nonetheless, it performs extremely well when it comes to dexterity, grasping and in-hand manipulation.

Overall, there are many approaches and morphologies possible when designing robotic hands and many successfully exhibit high dexterity. For this reason, this project does not focus on the hand design itself but on how the current solutions can be improved. It seems that the use of soft materials is a step in the right direction, enabling the passive non-linear responses observed in human hands. It improves grasp stability or actuation (in the case of a pneumatic system) while not hindering the range of motion of the system. It also appears that there is a lack of sensor integration in these designs, thereby reducing their potential applications. This is the problem tackled by this project: combining soft materials and sensing by creating a glove-like skin which can be customised and fitted onto any existing robotic hand.



Figure 2.1: Anthropomorphic hand implementations, from left to right: TUAT hand [14], Xu’s highly anthropomorphic hand [11], and BCL-26 soft robotic hand [5].

2.2 Sensors

For a robotic hand, tactile sensing technologies greatly facilitates the control as it provides a direct feedback mechanism to the robotic system or user. A comprehensible review of existing sensing technologies can be found in [9]. This paper details the most common approaches to tactile sensing and describes how each is integrated in robotic hands and haptic applications, highlighting that there should be a focus on interpreting the sensor data in order to achieve dexterous solutions. An overview of the different control algorithms is also provided for each application. From such reviews it appears that the use of air pockets embedded in a soft skin and connected to pressure sensors is a sensing technology that remains unexplored. This section examines the main sensing implementation for robotic manipulation problems, comparing them to assess the key characteristics our sensorised skin should possess.

Vision systems are often used alongside robotic manipulators [15], [16]. An advantage of such external system is the fact that there is no need to integrate them in the design of the robot or its manufacturing process. However, for many dexterous manipulation tasks, this provides insufficient information if they involve high amounts of occlusion for example during in-hand manipulation, exploration in low-light, tasks handling deformable objects and discovering texture [17]. To circumvent this, optical sensing can be embedded within the soft material such as presented in [18], [19] and measures the deformation of the gripper surface to infer force or slippage. However, this approach imposes many constraints when designing and manufacturing the hand. Another way to keep the sensing separate from the manufacturing of the robotic hand is to add a glove-like sensor array made out of flexible fabric [20], however this results in a material constraint on the surface of the gripper. As highlighted in the previous section this may be undesirable if high deformation or friction is required to improve grasp stability.

There are many different types of tactile sensors, and most rely on hard components (e.g., piezoresistive, capacitive, piezoelectric, optical) which are unsuitable for soft robotic hands [9, 21]. By definition, directly placing these sensors on a robotic hand results in the removal of a fully soft response. For this reason, soft sensing is an emerging field [22]

with developments including soft strain sensors [23], liquid metal (EGaIn) [24, 25], self-healing ionic hydrogels [26], and acoustic sensing [27]. Barometric sensors in direct contact with a silicone rubber [28] have previously been shown to have good sensitivity although lower frequency response. Another partially soft sensorised skin solution can be achieved by embedding small magnets in a silicon skin and placing hall sensors underneath [29], however the sensor density is limited to a single sensor per fingertip.

Multi-modal sensing [30], [31] and [32] is also a distinctive approach for complex applications. However, such solutions often require components of higher complexity and price and impose limitations on the design and integration with robotic systems. While all these show promise, there are limitations in receptor density, electronic readout, and non-linear, time varying responses [33].

There are several crucial parameters which one should take into account when selecting a sensor for tactile feedback in robotic manipulation. In [9], the authors discuss the task related requirements for in-hand manipulation. This includes locating and measuring contact forces, detecting surface properties and detecting slip detection to estimate grip stability. The selection of sensors is also very task dependent and there are few characteristics to consider during design stages. Spatial resolution should be high for in-hand manipulation tasks [34]. In a similar way to human's numerous nerve endings, high resolution enables the detection of smaller contact points and textures. High sensitivity, the ability to detect small variations in pressure is also desirable, especially when manipulating fragile or deformable objects. A high frequency response can be useful when attempting to detect vibrations or slippage [35]. Achieving low hysteresis is often difficult with soft materials and is important to achieve better dynamic responses and simplify data interpretation [36]. Finally having a low number of wire connections is always preferable to reduce the integration challenge [37] and a high surface friction to reduce the normal forces when grasping is preferred to avoid slippage. This falls into the material selection process which should further take into account robustness and flexibility. All of the aforementioned is re-considered when discussing the results obtained from the sensorised skin of this project

2.3 Materials

A major aspect when designing soft robots is the materials used. For tactile applications, the material forming the outer layer of the skin is of the upmost importance as it defines how the robot is able to interact with its environment. As mentioned in the previous section, using soft materials increases possible hysteresis [38] which is undesirable for repeatability in interactions. This is further accentuated by elastic materials which may experience plastic deformation if under high strain or as the material ages. The use of soft materials also reduce the frequency response and operating bandwidth of embedded

sensors. Wear and tear is an issue for soft materials which typically have a lower hardness than the objects they interact with. Using more durable materials like hard rubbers however results in reduced friction and soft properties. An alternative is to use self-healing materials [39], in a similar way to what human skin does. However, such technology is in its early stages of research and currently the properties of such materials are no match for those of non-healing materials when it comes to elasticity or friction.

The two fundamental features of soft materials are the embedded compliancy and the improved coefficient of friction. If the coefficient of friction was too low, a large normal force would be required to prevent object from slipping and this can result in the object breaking under pressure [40]. On the other hand, a high coefficient of friction is problematic for tactile exploration tasks [41], for example when attempting to slide a finger along a surface to feel its texture. Overall, the material selection is highly dependent on the tasks and requires various trade offs between different properties.

2.4 Modelling and Data Interpretation

Modelling and simulating the behaviour of a robot is a very powerful tool as experiments can be run many times much faster than in real life. It can also help reduce the number of prototypes in the iterative process of designing a robotic system. In this project, there are two things which can be modelled. The first is the kinematics of the hand used to control the finger actuation, this has been considered in the past [42] and this project focuses on sensor integration rather than control so it isn't further investigated. The second behaviour which may be of interest to simulate is the soft sensors' response to interactions, enabling better data interpretation and improved sensor design. Barometric sensors arguably behave in the opposite fashion to pneumatic actuators, a well-studied and simulate problem. The air chamber's deformation leads to a change in pressure while soft pneumatic actuators deform under a change in internal pressure. This section focuses on the modelling approaches used by other researchers in the field of soft robotics.

Modelling and simulating the behaviour of a robot is an efficient tool but a soft robot's kinematics often do not have a simple analytical solutions. When it comes to modelling soft robots, it is typically divided into two categories, model-based or model-free. Modelled based approach all rely on a simplification of the system's internal dynamics so that it becomes discrete entities for which classical motion analysis can be performed. This includes finite element analysis (FEA) [43] and voxels approximations [44]. Issues with these methods include the high computational cost and difficulty to replicate specific material behaviours, leading to sim-to-real transferability problems as detailed in [45]. Depending on the robot properties, an even simpler approach can be to reduce the number of degrees of freedom and simulate it like a chain of rigid bodies. A loss of accuracy is to be expected when simulating a reduced order system but this can be compensated by the

natural compliancy of the system.

Model-free approaches typically include data-based reinforcement learning approaches. Large datasets are used to train a universal approximator which models the complex dynamic behaviours and interactions of soft robots. There exist systems which self-model [46] by recording many action-sensation pairs (e.g. through motor babbling), but this requires additional state sensors. In [23], the author trains a LSTM network to map the strain sensor information to robot state. The use of deep learning is described in [47] to estimate the location and magnitude of contact pressure forces in microchannel fluidic sensors embedded in an elastomer matrix. Since the deformation of soft components is complex and impractical to simulate [47], data interpretation can also be aided by LSTM-type networks, which are particularly suited to model non-linear and dynamical systems [48] with time dependencies and hysteresis. Another approach consists in bypassing modelling by mapping directly sensor inputs to in-hand manipulation tasks [49], creating a robust closed-loop feedback controller. The use of neural networks is a solution many seem to use for data interpretation or control and has so far shown promising results for diverse applications.

2.5 Control

Once a robot is built, it needs to be controlled and for soft robots this is another challenge as described in this review [45]. Kinematic and dynamic models are only ever approximations, leading to issues of stability when attempting to transfer from simulation to physical systems. Mapping directly the sensor inputs to in-hand manipulation tasks without analytic dynamics has the benefit of creating a robust closed-loop feedback controller [49]. However, this solution is often limited to a single set of similar tasks, a model needs to be re-trained with new data to achieve stable control of another task. More complex systems can combine multiple controllers, as shown in [50]. In-hand manipulation is achieved by hierarchical decomposition using a high-level controller based on reinforcement learning and a low-level policy which relies on tactile sensors. Methods known from image processing [41], [51] in combination with PID-type controllers [52] can also be used for tactile servoing, precise position control and manipulation tasks. The latter paper describes the use of a deep tactile Model Predictive Controller to perform tactile servoing directly from the high resolution sensor data of the GelSight sensor [53].

2.6 Previous Work

The hardware used for this project is predominantly from past projects of the PhD student Kieran Gilday. Details on the hardware manufacturing and its usage for this project is

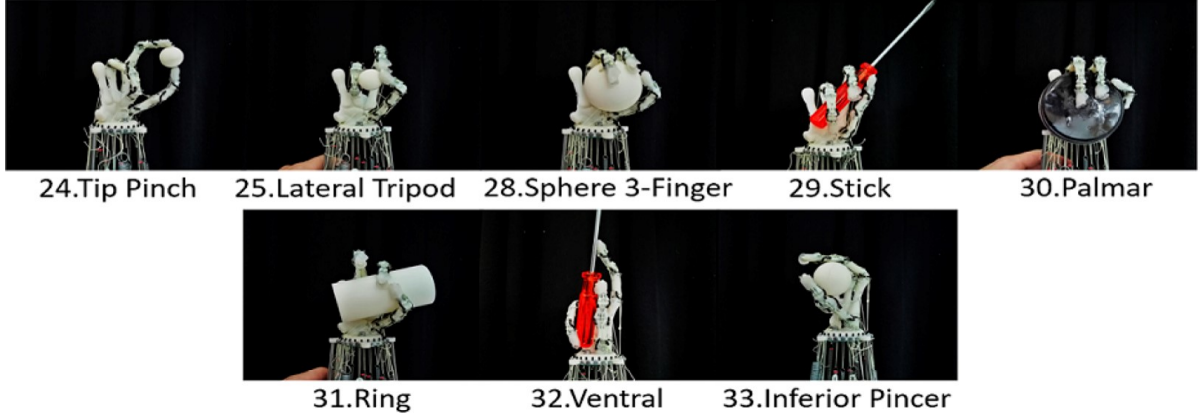


Figure 2.2: Anthropomorphic skeleton from [42] and [54] for hand used in this project shown to achieve example grasp types from the GRASP taxonomy (Image from [54]).

discussed in the following chapter. This section briefly describes what has been achieved in the past with the anthropomorphic hand previously developed.

The first research focused on a vision-based system, which looks at the tendon displacements to estimate changes in posture of the hand and external forces through a kinematic model of each finger [42]. This low-cost, scalable approach to sensing also has the advantage of not interfering with the hand dynamics and its design. In [54], the authors detail the manufacturing process of the skeleton-like hand designed. It then performs passive grasping by adapting wrist trajectories, demonstrating the potential of compliant designs for generalised and transferable grasping.

In this project, the same skeletal structure is used as the base of the anthropomorphic hand. It is shown in Figure 2.2, passively achieving different precision grasps. On top of it is added the soft sensorised skin for which no characterisation results were previously produced.

Chapter 3

Experimental Apparatus and Methods

3.1 Sensorised Skin Manufacturing

This section provides a description of the manufacturing of the soft sensorised skin. In depth details regarding the manufacturing of the tendon-driven skeleton are included in [54]. The sensing relies on air chambers embedded in the skin and connected to external pressure sensors. The skin is cast as one part and later fitted onto the existing anatomical hand like a glove. Figure 3.1 shows how and where the air chambers are embedded within the skin. A specialised mold is created, consisting of three main sections: the inner skeleton mold, the chamber molds and the overall hand mold. Individual sensing chambers can be placed around the skeleton, tailored to needs. Figure 3.1 shows three chamber molds, for the thumb, index and middle finger; each of these finger has 10 chambers distributed along their length. This includes six sensing chambers in each fingertip, and two sensors at each of the PIP and MCP joints. An additional two air chambers are placed within the palm for a total of 32 chambers in this design. The air chambers are located close to the surface, for higher sensitivity, and wrap around the side of the finger, for insertion of pneumatic tubing, Figure 3.3.

The fabrication process can be broken up into two main stages, the skin molding (Figure 3.2a and b) and the hand assembly (Figure 3.2c, d and e). The skeletal and hand molds are FFF 3D printed, the chamber molds are printed at high resolution with a Connex 500 polyjet printer. Once the mold assembled, Ecoflex 00-30 silicone is cast to form the soft skin which contains air chambers. The skin is then placed over the tendon-driven hand shown in Figure 3.2c (see [54] for detailed fabrication). Finally, the sensors are assembled by inserting flexible pneumatic tubing into each chamber and routing it to one of the 32 available pressure gauges which are mounted on the back of the hand.

The tendon-driven anatomical hand is re-configurable into different postures and stiff-

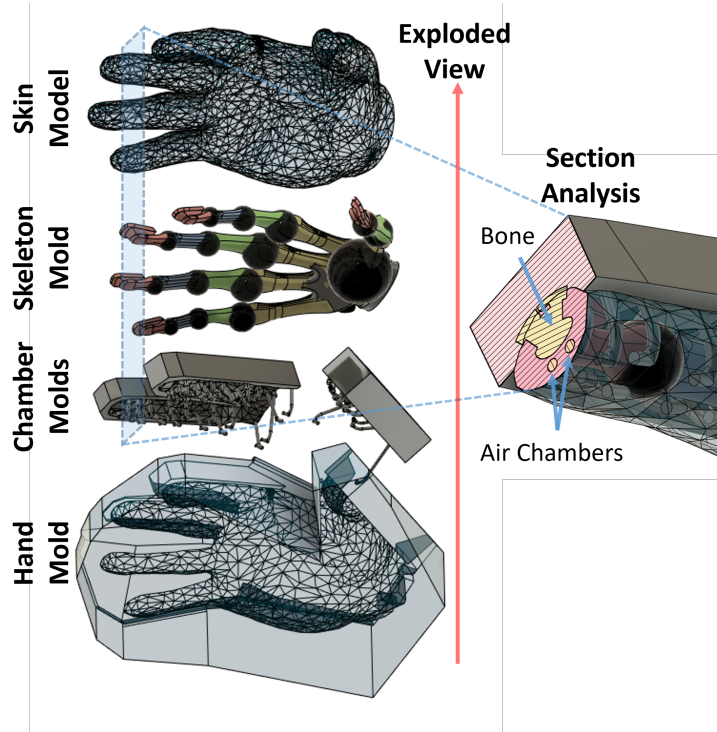


Figure 3.1: Sensorised hand and mold design. Exploded view shows the skin model (1st from top) and skeleton mold (2nd from top) used to make the hand skin mold (bottom). The created mold is then modified to add the custom air chambers in the desired locations (3rd from top). The section analysis shows a pair of air chambers in the middle fingertip.

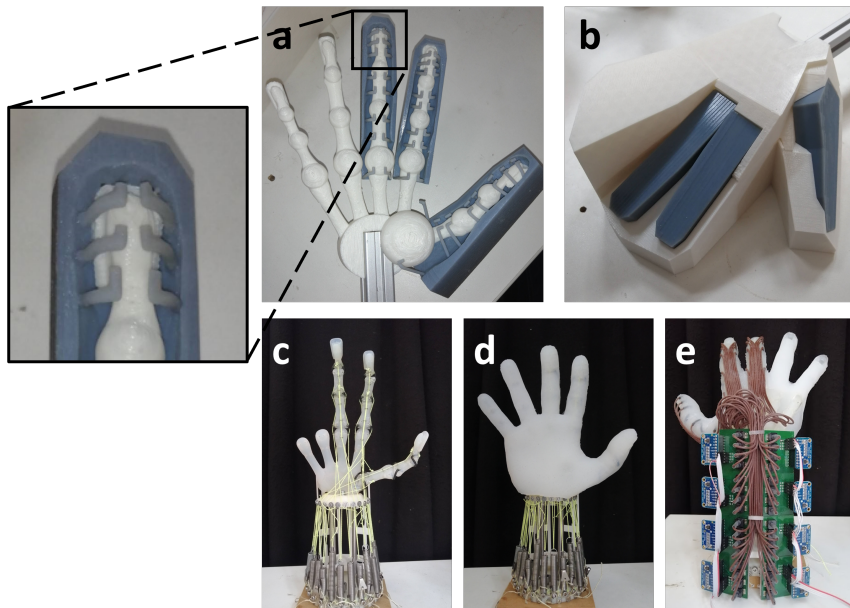


Figure 3.2: Sensorised hand fabrication. (a) Printed inner and chamber molds. (b) Fully assembled mold. (c) Tendon-driven, anatomical hand with thumb, index and middle finger. (d) Skin cast with Ecoflex 00-30 silicone. (e) Hand with 32 sensors, 10 in each finger (6 in fingertips), 2 in the palm.

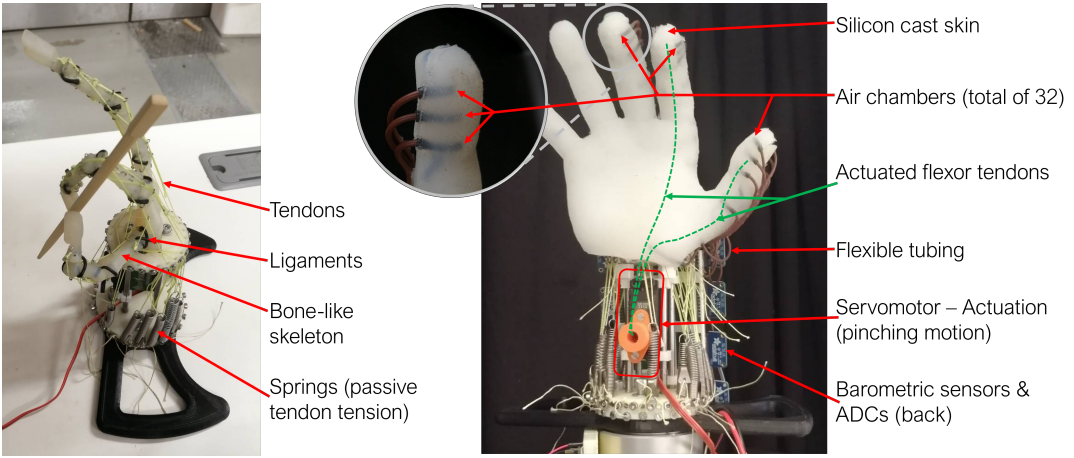


Figure 3.3: Annotated hand with sensorised skin and servomotor actuation mechanism.

nesses. A single servomotor was added inside of the wrist for actuation. Each finger has 5 tendons, the majority are connected to springs with tunable stiffness, the remaining can be flexed by the internal servo, for example to achieve a pinching motion by pulling on the flexor tendons of the thumb and index simultaneously. This is shown in Figure 3.3 along with a close up of a fingertip showing how the flexible tubing is inserted in the skin to reach the air chambers, connecting them to the pressure sensors.

3.2 System Framework

The sensing skin is based on a set of pressure gauges (NXP MPXH6300AC6U). These are surface mount components (PCB fixed to the back of the hand as shown in Figure 3.2e) which produce a voltage proportional to the barometric gauge pressure. This voltage is then read and transmitted by a 16-bit analog to digital converter (Adafruit ADS1115) at 860 samples/second over serial. By using a I²C bus, the number of wires and connections is reduced, with up to 16 sensors on each bus. Each pressure gauge is connected to an air chamber within the skin, using flexible silicone tubing. When skin is touched near to the chamber, deformation occurs causing a change in pressure following the ideal gas law. The chambers can be any shape. Different shapes can deform in different ways to tactile stimuli, so shapes can be tuned for localised sensing, large-area sensing, texture or internal bending. A simple elbow shape with 2mm tube thickness is selected for ease of manufacture, good sensor packing density and fingertip coverage.

The existing hand and software were modified (from [54]) to create a framework that can be used to perform a range of manipulation experiments. A servomotor was added to actuate the index and thumb to produce a suitable motion for pinching tasks. The servomotor and sensors are both connected to a central computer through a microcontroller as shown in Figure 3.4. The hand is mounted at the end of a UR5 robot arm which is used for the manipulation tasks described in the following sections. The software architecture

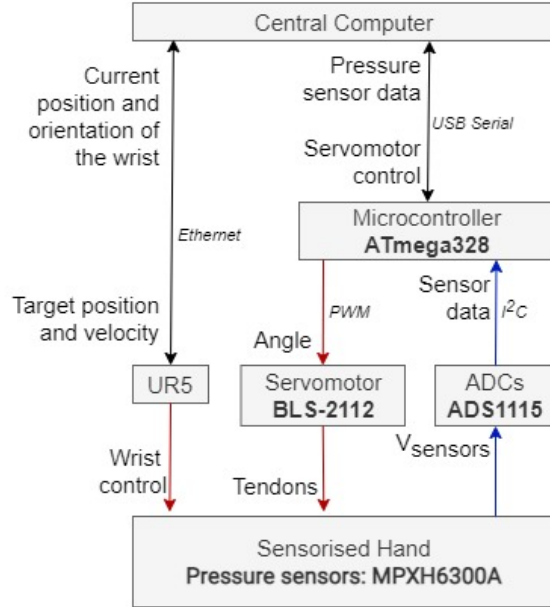


Figure 3.4: Overall framework diagram presenting experimental setup and connections between modules.

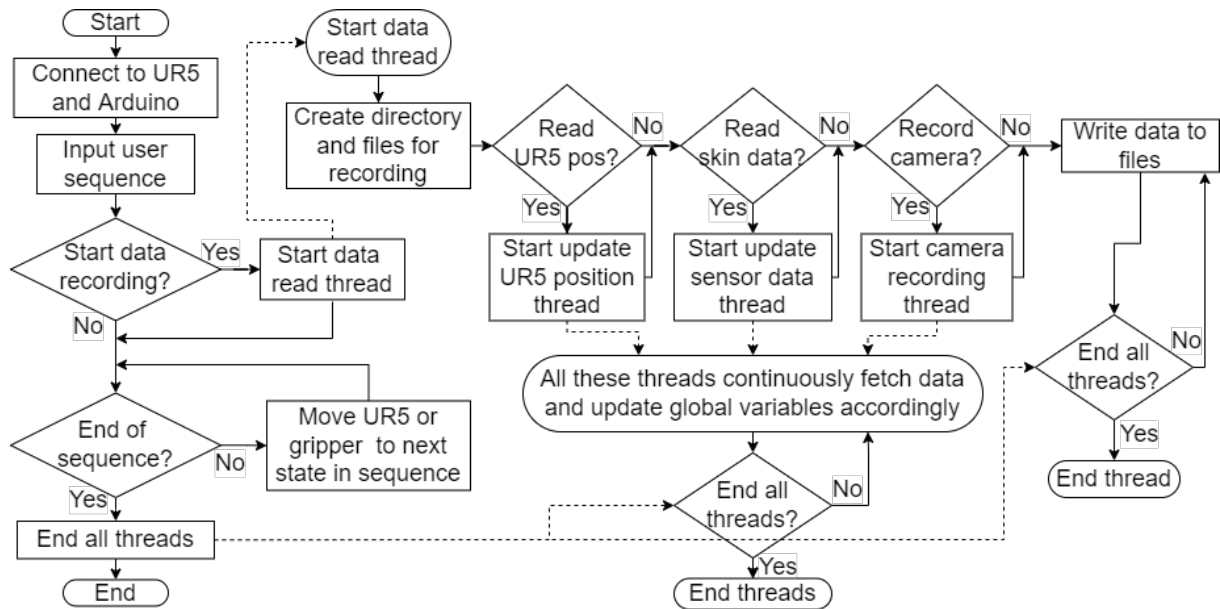


Figure 3.5: Flowchart of software implementation for open-loop controller for data collection experiments.

for the open-loop experiments is described in the flowchart shown in Figure 3.5. The central computer first initiates a connection with the UR5 arm and the microcontroller, in this case an Arduino Nano, which is connected to the sensors and servomotor. It then performs a predefined motion sequence for the arm and hand, by controlling the UR5 and servomotor position and velocity. If required it starts a simultaneous data recording thread which in turn starts parallel threads for each type of data that should be recorded.

This includes recording the UR5 position, raw skin data or an external camera input. Finally at the end of the pre-programmed motion, all threads are ended. For close-loop control, the difference in architecture is that the robot motion isn't fixed at the start of the experiment but updated depending on sensor data.

3.3 Sensor Characterisation

This section discusses the experimental method which was used to characterise the sensors. The investigated characteristics include long and short term response (i.e. hysteresis), repeatability, sensitivity and the varying pressure response with changes in air chamber shape, indent tool and distance to sensor.

The first experiment is the characterisation of the time response, long and short-term, of a single sensor using controlled motions as depicted in Figure 3.4. The hand and fingertip position can be controlled to stimulate a single sensor by contacting with the environment. Robot location and orientation data is obtained from the inverse kinematics of the UR5, sampled synchronously with the sensor data. Sensor data is read by an Arduino from individual analog to digital converters (ADCs) and recorded by the central computer at 20Hz for 16 sensors. With a rapid step motion (< 10ms), the transient response of a single sensor using a faster sampling rate, 62.6Hz, can be observed. With press and hold motion, any decay in sensor reading over time is observable. With a repetitive motion the

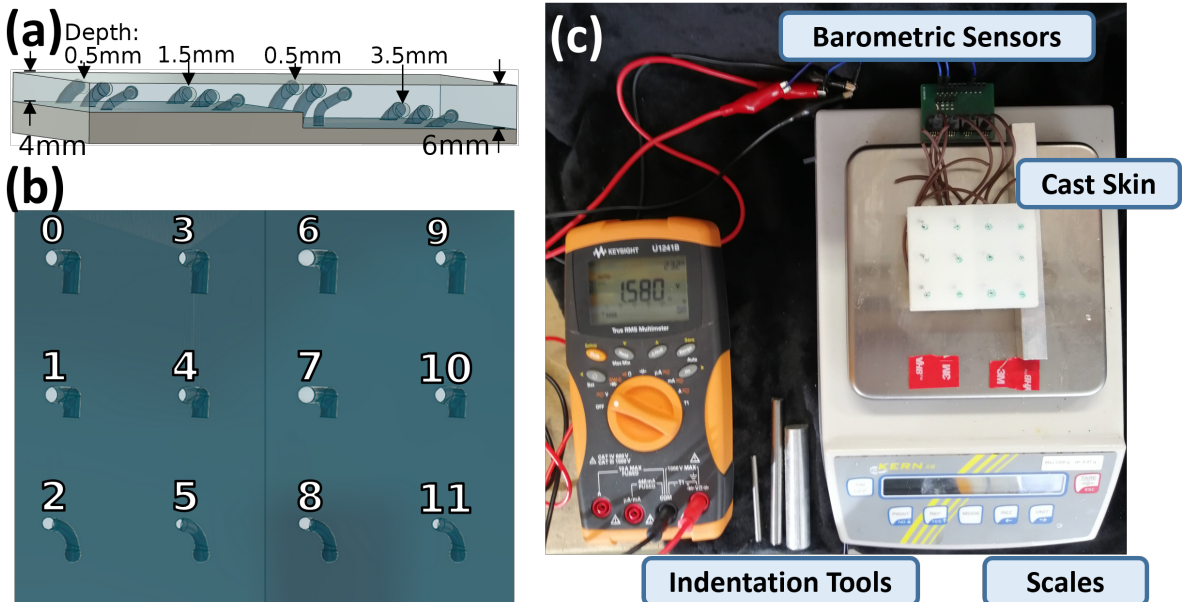


Figure 3.6: (a) Sample skin dimensions: distance between air chamber and surface of the skin (depth) and total skin thickness. (b) Labelled sensor samples. Each column is placed the same way in the skin, each row is a different receptor design, top to bottom: long elbow, short elbow, spherical. (c) Experimental setup for measuring sensor response under controlled loads.

repeatability of sensor response is examined. The results are discussed in the following chapter.

To test air chamber shapes and sensitivity, a separate sample skin was manufactured with twelve air chambers which have varying designs and depths under the skin surface, as shown in Figure 3.6. Air chambers are grouped by skin thickness and depth (e.g. receptors 0-2 at 4mm thickness and 0.5mm depth) or by type: long elbow (0,3,6,9), short elbow or spherical, Figure 3.6b. The molded sample skin is glued to a printed base and flexible tubing connects the start of the chambers to pressure sensors the same way as the anthropomorphic skin. Figure 3.6c shows the experimental setup used to characterise this skin sample. The sample is placed on a set of scales and the flexible tubing is connected to the pressure sensors and read by a voltmeter. Three indenting tools are selected, cylinders with diameters 4, 8 and 15mm. Tools can be pressed manually onto each air chamber. Varying the tools and applied force (measured using the scales), sensitivity to force distribution can be measured. Varying the distance between the indenting force and air chamber, sensitivity to force localisation can be measured. Varying the force to observe the lowest sensor voltage detected with the voltmeter and the highest force before no voltage change is detected, sensor ranges can be measured.

3.4 Tool Manipulation and Sensing Experiments

This section discusses the experimental methods for tasks involving the use of the anthropomorphic hand and soft sensorised skin. The following three experiments show how data interpretation can be achieved and used for feedback control.

3.4.1 Picking

Picking is a very common problem in robotics and a task humans unconsciously repeat many times on a daily basis. It is arguably the most common and necessary of all manipulation tasks. It is also the first step to any manipulation or tool use. For these reasons, achieving open-loop picking using the hand previously manufactured is the first experiment implemented. The actuation mechanism relies on a single servomotor coupled to two parallel 3d printed pulleys on which the index and thumb flexor tendons are attached. By actuating the servomotor, the two fingers move towards each other in a pinch-like motion, allowing the hand to actively pick up and grasp a range of objects.

This experiment looks at the data provided by the tactile system while repeatedly picking a single object to investigate the possibility of data interpretation by observing emerging patterns. To do this, successive pickings are performed with and without a thin cylindrical object, for example a chopstick. The experimental setup consisted in a chopstick positioned between two v-shaped holders. The hand is lowered, pinches the

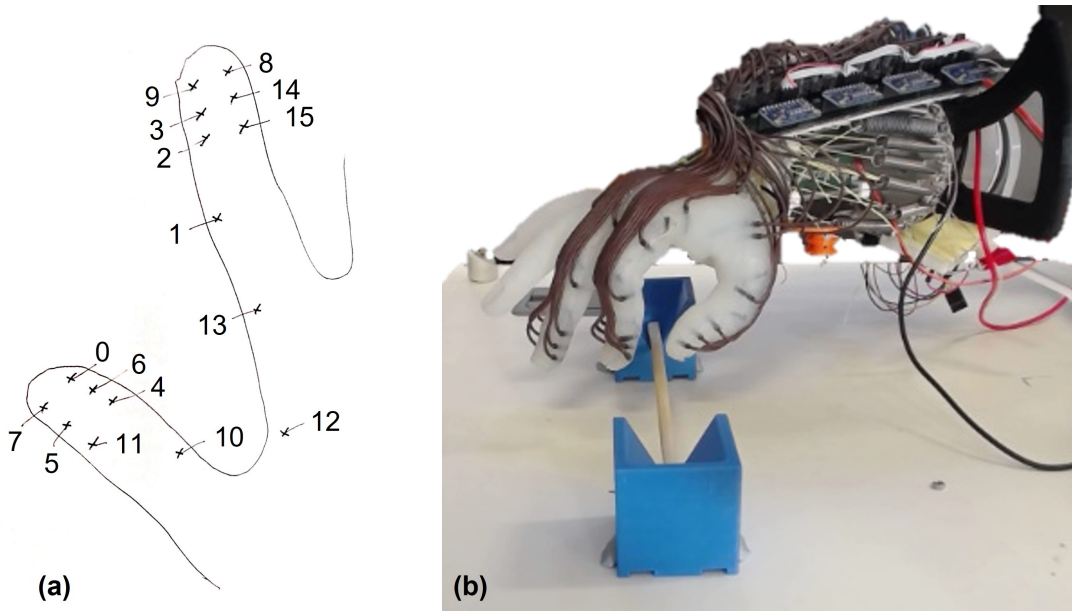


Figure 3.7: (a) Air chamber locations in skin for 16 sensors used. (b) Experimental setup used for pinching data collection. Example of picking with a chopstick.

chopstick, lifts it, drops it and repeats this for 100 iterations. The v-shaped holders ensured that the chopstick always fell back in its original position to ensure repeatable initial conditions throughout the experiment. The setup is shown in Figure 3.7(b). The same experiment can then be repeated without a chopstick to observe how an object can create a specific sensor image. If there is a noticeable difference in response, it is possible to conclude that data interpretation and feedback control are possible.

For the following experiments, 16 air chamber locations were selected and connected to pressure sensors on one of the I^2C buses. The selected chambers are shown in Figure 3.7(a). When performing pinching tasks, the sensors most likely to observe a response are the ones in the index and thumb fingertips, justifying 12 of the selected chambers. Because these fingers are actuated and could bend, an additional 4 chambers along the length of the thumb and index were connected to the remaining available pressure sensors.

3.4.2 Orientation Prediction with Neural Networks

Having showed that data interpretation is possible for a simple picking task, it must now be implemented. The following step in tool use is manipulation which requires understanding contacts and interactions. As explained in the literature review, modelling the soft skin and it's response to environment interactions is complex for several reasons. The complexity of the skin and air chamber shapes are hard to simulate and the current modelling technologies do not provide simple and cost effective solutions to facilitate data interpretation and control. For these reasons, this project shows how a model-free approach based on training neural networks for a specific task can enable mapping sensor

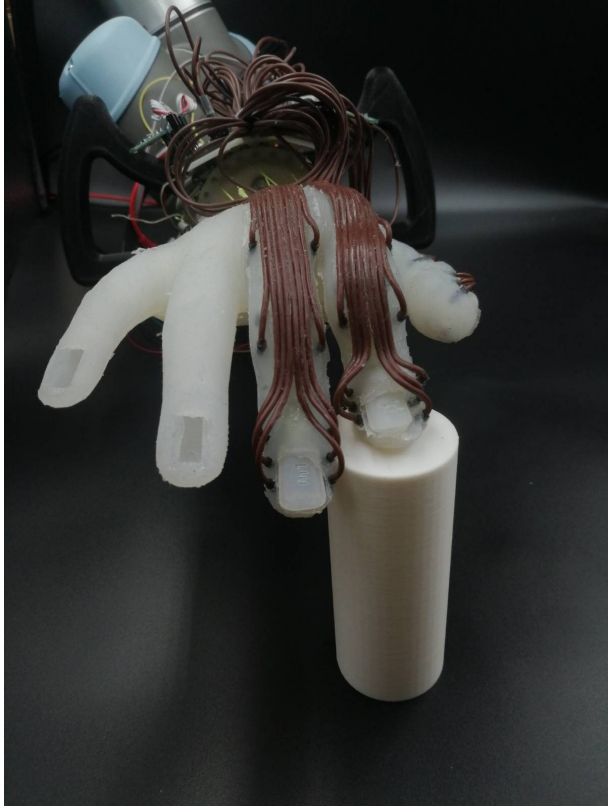


Figure 3.8: Experimental setup for data collection of wrist orientation data and tactile fingertip data.

inputs to robot states.

A common haptic and robotic problem is the knowledge of a surface's orientation with respect to the end effector [55]. This challenge is accentuated by soft robotic systems because of their underactuated forward kinematic models and the complexity associated with the integration of hard sensors. Knowing surface orientation is key for exploration and in-hand manipulation algorithms which require accurate surface reconstruction. Using an array of 6 air chambers in a single fingertip (Figure 3.2, zoomed in image), it is possible to reconstruct the relative positioning of the hand with respect to a flat surface. This is achieved by collecting data from the fingertip sensors along with hand rotations from the UR5 and training different types of neural networks to map the highly dimensional sensor inputs to robot positions. To collect said data, the index fingertip was kept in constant contact with the flat surface and the hand rotated about all 3-axes around the center of the fingertip, using the UR5 arm. During this motion, the sensor readings and orientation data, from the UR5's built-in inverse kinematics solver, were continuously recorded with data sampling rate 20Hz, creating suitable training and testing datasets. The setup for this experiment is shown in Figure 3.8.

This experiment relies on machine learning to create an abstract model which maps the sensor data inputs to the relative orientation between a fingertip and flat surface. Following the Universal Approximation Theorem, neural networks can approximate any

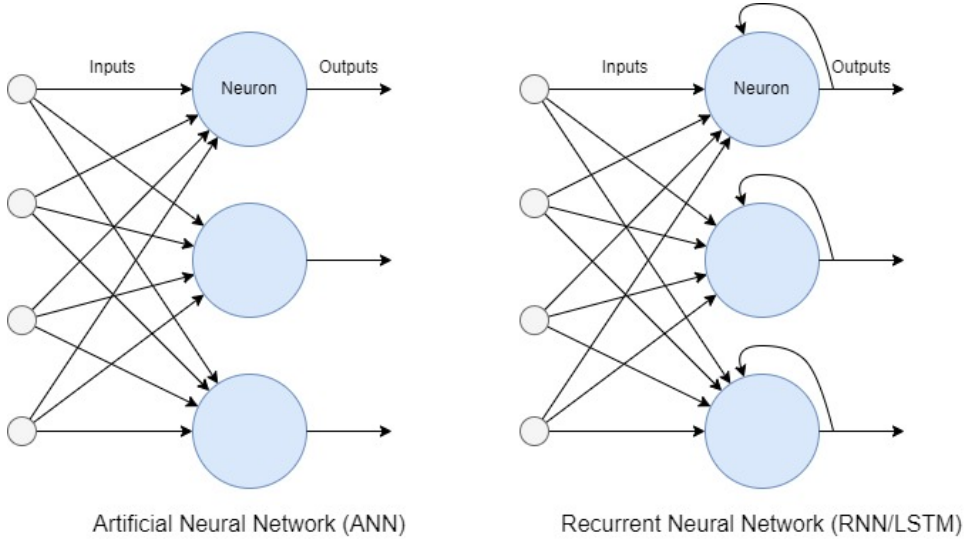


Figure 3.9: Comparaison of ANNs and RNNs (LSTM) topologies.

multidimensional function [56], which is the relationship between sensor inputs and hand orientation for this experiment. This project relies on deep neural networks for data interpretation. Such networks are inspired from the morphology and functioning of the brain, with interconnected layers of individual neurons. On an individual basis, neurons have many inputs that are weighted, summed and passed through an activation function to produce a single output. The outputs can then be fed in the following layers of the network or in previous layers as well for recurrent neural networks which model time dependencies in sequential data. The learning consists in optimisation of the weights through successive iterations using the training and testing datasets.

Two different types of networks were trained with identical data to analyse the impacts of network architecture. The first is a classic artificial neural network (ANN) and the second a long short-term memory network (LSTM), which is a subset of the recurrent neural network (RNN) type. ANNs are feed-forward networks only while LSTMs are able to model dynamical systems and therefore time dependencies in sequential data. This is achieved by feeding back the neuron outputs as inputs of the current or previous layers. Such topologies are shown in Figure 3.9. Exploring these different types of networks enables the analysis of the time dependencies caused by hysteresis in the soft materials used to evaluate their impact on the feasibility of data interpretation.

The network topologies, number and type of layers as well as other hyperparameters, are summarised in Figure 3.10 for each of the two networks implemented. These hyperparameters were determined empirically to minimise training time and reduce error. Neurons and layers were progressively added until no significant drop in loss was observed. The selected activation function was ReLU (Rectified Linear Unit) because of its popularity for such tasks and its computing efficiency, thereby reducing training time. The regression relied on a mean squared error loss function and the optimization algorithm

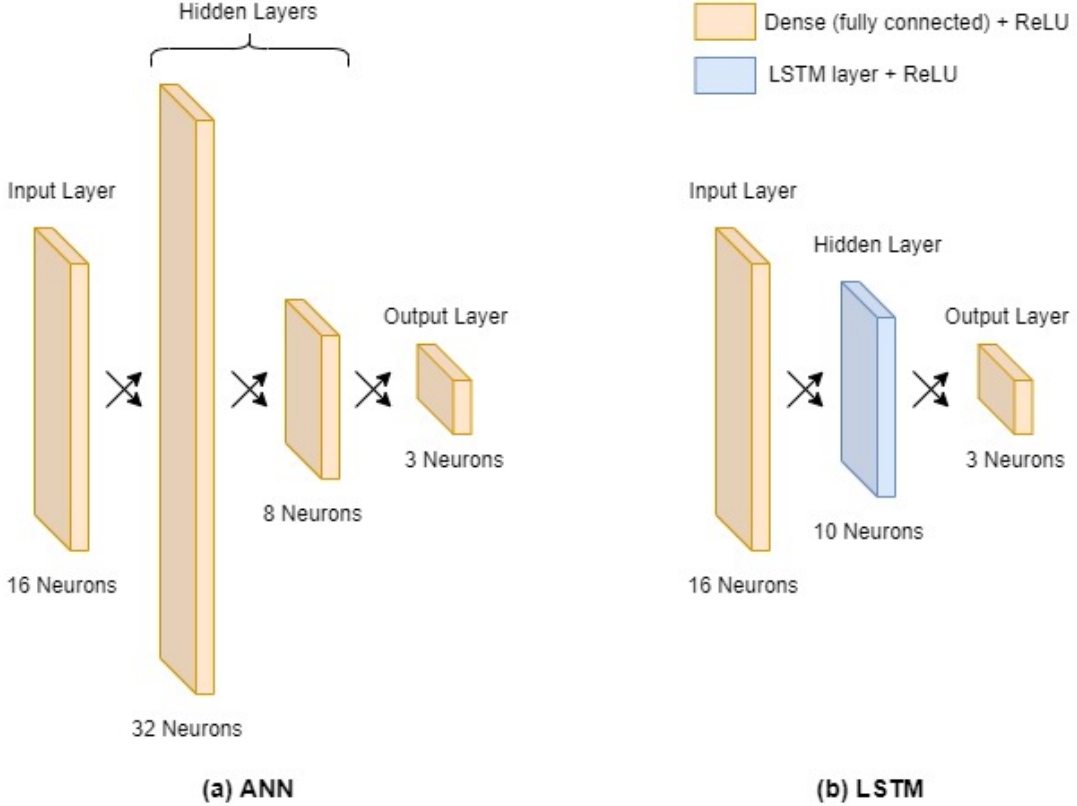


Figure 3.10: ANN and LSTM network architectures (layer types and sizes) used for hand orientation prediction from fingertip sensor data.

used for stochastic gradient descent was Adam (Adaptive Moment Estimation). This popular optimizer updates the weights and biases at each neuron when iteratively training the network.

The networks were implemented using the Python deep learning API Keras, an interface library for TensorFlow. This enables simple and rapid development using state-of-the-art systems.

3.4.3 Hole Detection and Peg-in-hole Problem

Following data interpretation for a single contact, the next step is to use a tool environment exploration and remote sensing. Tool manipulation is another typical problem in the field of robotics. Using tools enable a greater range of achievable tasks. This experiment shows how a tool (in this case a chopstick) can be used for remote sensing and detection of holes on a flat surface. A chopstick is placed manually in the hand and held in place in a pinching grasp by actuating the servo. The chopstick is then dragged over a series of holes with known diameter while the sensor and robot position data are recorded synchronously. This aim of this experiment is to emphasize that by knowing the sensitivity and controlling the relative positioning of sensors in the soft skin, simplified modelling of the tool interactions can be performed to predict what diameter hole the

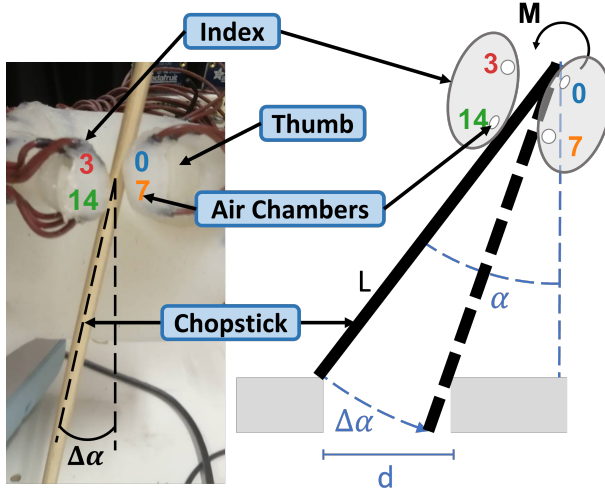


Figure 3.11: Model of fingertip sensor compression when the pinched chopstick is rotated by a certain angle $\Delta\alpha$. The compliancy of the soft skin and skeleton provides a restoring moment M . The right hand side sketch shows the model used to derive (3.1) for the hole detection problem (d is the diameter of the hole detected).

sensorised skin is able to detect. The setup for this experiment is shown in Figure 3.12.

To detect a hole when dragging a chopstick across it, the system must be able to detect a change in its angle. Two features of the design enable this detection. The first is the lateral placement of air chambers on each fingertip, which can capture information of the relative deformations in the skin introduced by a change in angle of the chopstick. The second is the compliancy of the soft skin and skeleton that provide a restoring moment which in turn compresses the air chambers, while allowing the chopstick to change angle when encountering a hole or obstacle, as shown in Figure 3.11.

Figure 3.11 demonstrates how the chopstick behaves when encountering a hole while being pinched between the index and thumb, which apply forces attempting to restore the chopstick in a vertical position. The moment created by the pinching induces a sudden jump in angle as the tip chopstick falls in the hole as it is dragged on a flat surface. The diameter (d) of the detectable hole size depends on the chopstick angle α as it is dragged and minimum sensor sensitivity, i.e. the minimum detectable angle $\Delta\alpha$. The diagram shown in Figure 3.11 is used to derive this relationship which is shown in Equation 3.1.

$$d = \sqrt{L^2 + \left(\frac{L \cdot \cos(\alpha)}{\cos(\alpha - \Delta\alpha)}\right)^2 - \frac{2 \cdot L^2 \cdot \cos(\alpha) \cdot \cos(\Delta\alpha)}{\cos(\alpha - \Delta\alpha)}} \quad (3.1)$$

To find the minimum detectable angle $\Delta\alpha$, the tip of a chopstick was attached to fixed pin joint while the other end was being pinched between the hand index and thumb. A UR5 arm was then used to incrementally increase the angle of the chopstick until the change can be reliably detected by skin sensors. Once $\Delta\alpha$ is obtained, it can be plugged into Equation 3.1 to obtain $d = f(\alpha)$. To assess the accuracy of this relationship,

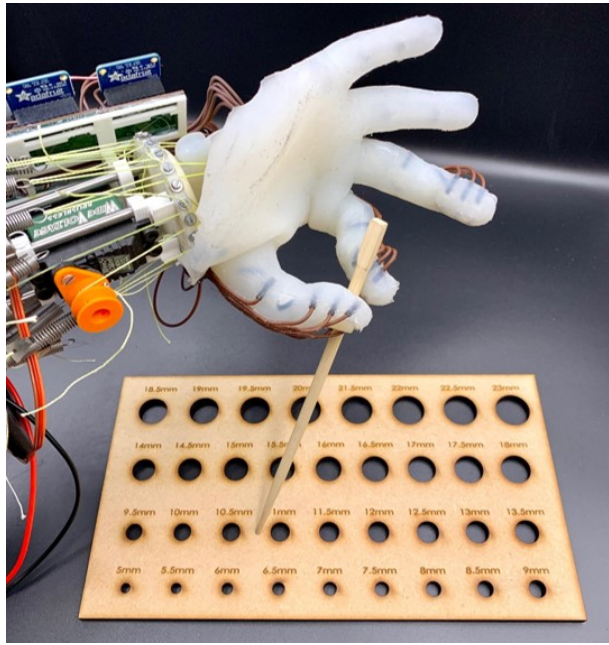


Figure 3.12: Experimental setup for hole detection on a flat surface using a chopstick as a tool for remote sensing. Chopstick is dragged across laser-cut board with varying size holes.

the chopstick can then be dragged across a laser-cut board with varying hole size to empirically confirm this aforementioned relationship. The setup for this experiment is shown in Figure 3.12. All results and discussion are presented in the following chapter

Chapter 4

Results and Discussion

4.1 Sensor Characterisation

In the first stages of experiments, the sensor characteristics were analysed to enable comparison with other existing sensing technologies. Figure 4.1 shows the results of varying tool size and indenting force on the measured pressure. Comparing changes in indenting force, increasing the force always increases the measured pressure, as expected. Though this increase is non-linear. Different receptor designs placed the same way in the skin can be compared (individual quadrants, e.g., sensors 0-2 compared to 3-4 in Figure 3.6). The long elbow design is the most sensitive for the smallest indenting tool (except for sensor 6, an outlier caused by leakage from manufacturing error). Increasing the size of the indenting tool decreases sensitivity, as expected since applied pressure to the receptor

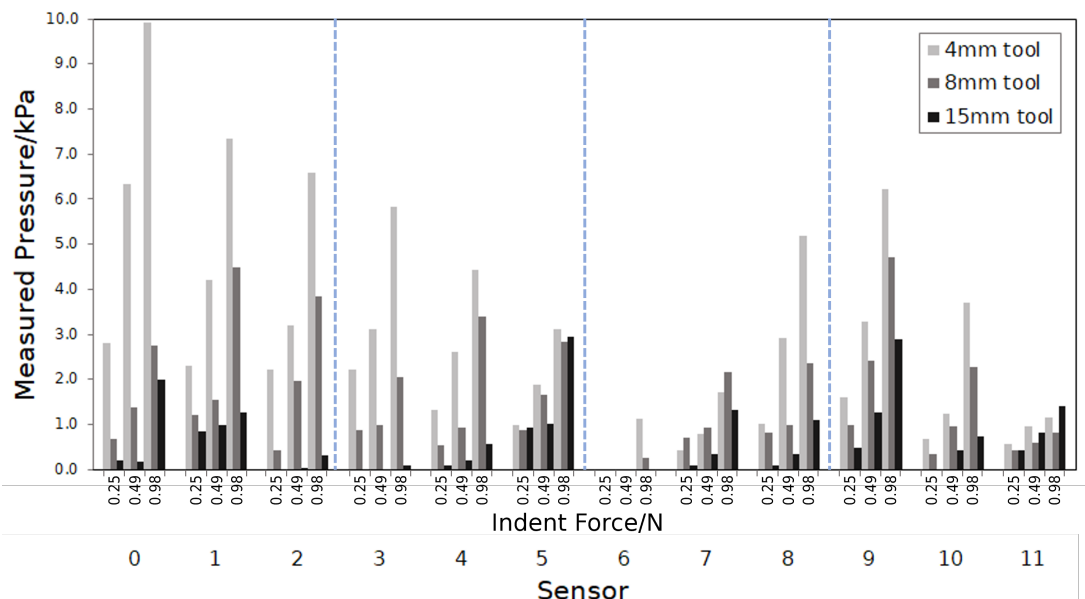


Figure 4.1: Results from skin sample tests, sensor number corresponds to Figure 3.6b. Measured sensor pressure with varying indent tool (4, 8, 15mm) and force (0.25, 0.49, 0.98N).

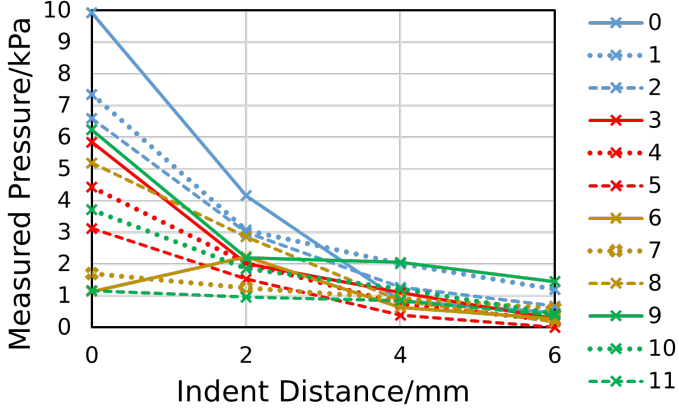


Figure 4.2: Results from skin sample tests, sensor number corresponds to Figure 3.6b. Measured sensor pressure against distance from sensor centre for a constant force (0.98N) and indent tool (4mm).

Table 4.1: Minimum and maximum forces observable with a voltmeter and the 4mm impressioning tool for sensors 0 and 11.

Sensor	$\Delta V_{min}/\text{mV}$	F_{min}/mN	$\Delta V_{max}/\text{mV}$	F_{max}/mN
0	1 ± 0.5	23 ± 6	172 ± 1	1600 ± 200
11	1 ± 0.5	59 ± 20	132 ± 0.5	5700 ± 90

is reduced. Receptors placed deeper in the skin are less sensitive (comparing set 0-2 to 3-5, or 6-8 to 9-11), though there is increase in sensitivity to the larger indenting tool in the spherical design (2 and 8 against 5 and 11). This means sensitivity to different stimuli can be controlled, for example, to detect large area forces, deeper and spherical shaped sensors are better.

Figure 4.2 shows the sensor response to changing the distance of the 4mm indenting tool to the centre of the receptor. For each receptor there is a rapid decay in sensitivity when moving a short distance from the centres. Every receptor, except for 5, retains some sensitivity at 6mm away (-3mm overlap between tool and sensor), and skin depth or thickness don't appear to have a significant effect outside of previously measured sensitivity differences (Figure 4.1).

Table 4.1 shows force sensitivity and range test results. From the sensors in Figure 4.1, the apparent most and least sensitive to the 4mm indenting tool were selected, sensors 0 and 11 respectively. Sensor 0 has the largest volume, closest to the surface, so is expected to exhibit the greatest pressure change with the same force, whereas sensor 11 has the smallest volume, deepest under the surface. In this test, the tool is pressed directly onto each sensor until the minimum (from voltmeter resolution) or maximum (from sensor pressure saturation) observable change in voltage is observed. The smallest detectable force using this method is 23mN with sensor 0. With lower sensitivity, sensor 11 has a higher force range of $\approx 5700\text{mN}$. Sensitivity is given by the range of voltage over the range

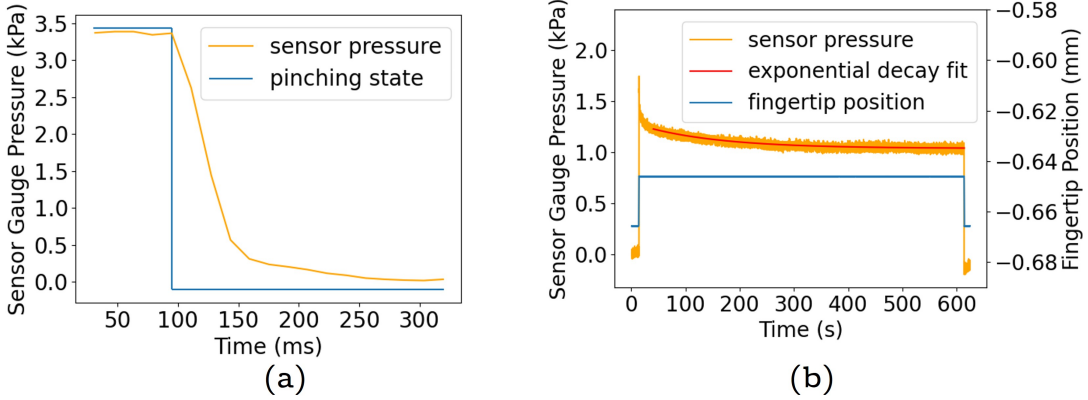


Figure 4.3: (a) Short term step response of a single sensor as hand opens from pinching grasp. (b) Long-term step response of a single sensor pressed against surface.

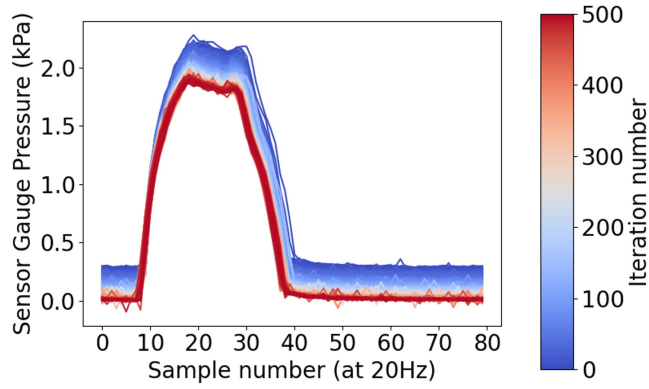


Figure 4.4: Repeatability of 500 successive contact between index fingertip and surface for a single sensor.

of force, $0.11V/N$ for sensor 0 and $0.023V/N$ for sensor 11. Resolution depends on the readout electronics and individual sensitivity. The theoretical minimum, based-on sensor 0 and a 16-bit ADC, is $0.69mN$.

Figure 4.3 shows the results of the single sensor time response experiments, as described in Section 3.3. Figure 4.3a shows a sensor step response from a pressed state to a released state. The pressure takes 50ms to recover, with no transient oscillations. This is a 20Hz bandwidth. It could be improved by casting the skin with a harder material; as the frequency response is limited by softness. A delay is expected for the step to cause a change in the pressure reading from propagation of the pressure wave, though for a 20cm sensor tube at atmospheric pressure, the delay is only 0.6ms, too small to be observed at this sampling rate. The speed of release of the pinch state is arguably also a limiting factor. The short time frame and the fact that it is impossible to visually tell if the sensor is still being compressed means that the current bandwidth measurement is a lower bound, the sensor response may be limited by how fast the pinching state changes. To improve results, the motion should be controlled by a much faster actuator than the servomotor or UR5, for example using a linear solenoid actuator which have retraction times reaching

2ms [57].

Air leaks in the sensors can cause rapid decay of signals. When manufacturing by hand there are inevitably manufacturing errors, though there may also be much smaller leaks from small defects or porosity in the materials. Figure 4.3b shows an example of this, a receptor is pressed for 10 minutes and released. The signal first jumps to a high pressure value before showing signs of decay. A drop lower than the initial atmospheric pressure value is also observed at the end, suggesting a negative pressure differential as the air chambers re-expand. This decay is very predictable, as seen in Figure 4.3(b)'s exponential fit (Decay time constant: $\tau = 143\text{s}$ and coefficient of determination: $R^2 = 0.88$), so it can be accounted for when implementing a controller.

Figure 4.4 shows the repeatability of the sensors. Ideally, after long term use, the sensor response should remain the same for the same stimuli. Here, a UR5 arm is used to repeatedly press and release the index fingertip against a flat surface. The colormap compares the response of 500 tests (80 samples, 4s each), measured over a total of 33 minutes. There is no degradation of performance or long-term plastic changes to the sensors under these conditions. The average transient decay observed is contained in the first half of the iterations; it's explained by the phenomena described in Figure 4.3b.

The main characteristics of the proposed sensor are summarised in Table 4.2 and compared with implementations from technologies mentioned in the literature review. Within a sensor category, there are many implementations with differing capabilities. A detailed review can be found in [9]. This table includes one example for each of the categories. As shown in the table, the bandwidth is lower than tactile sensing involving hard components. This is to be expected from an approach involving soft components. Resolution is very good, air chambers measure 2mm and could realistically be packed with a resolution of up to 3mm. The main drawback becomes the number of flexible tubes required when the number of chamber increases. Sensitivity and force range are both mid-range for this sensor.

Overall, this characterisation tells us the individual sensors can have excellent performance, with bandwidth up to 20Hz, detectable forces as small as 23mN, repeatability, localisation within -3mm overlap, and potential to control response to stimuli through

Table 4.2: Sensor characterisation results summary and comparison with other tactile sensors.

Sensor Type	Bandwidth (Hz)	Res. (mm)	Sensitivity (mN)	Range (N)
Piezoresistive [58]	1000	5	200	20
Capacitive [59]	24.4	4	6.25	7kPa
Barometric [38]	50	5	10	4.9
Optical tactile [60]	10	3	80	1.8
Our approach	20	3	23	5.7

placement within the skin and receptor design. However, there are significant variations in sensitivity and behaviour which may originate from manufacturing defects and inhomogeneities in the skin. Therefore, data extraction is more challenging when using a model-based approach. Some data-driven approaches are potentially well suited, however.

4.2 Tool Manipulation and Sensing Experiments

4.2.1 Picking

This experiment was done as an introductory step to data interpretation. If there are noticeable patterns for very simple use cases, it suggests that data from more complex tasks likely also contains underlying patterns, even if hard to observe visually. As mentioned in the previous section, the selected task is picking of a thin cylindrical rod, a chopstick. Results for the comparison of sensor data with and without chopstick are shown in Figure 4.5.

The data for each sensor was normalised by removing the average of the measured values when the hand isn't pinching. The error bars show the range of the measured data during picking, when the fingertips are in contact with each other or the chopstick. Figure 4.5 shows that there is a clear difference between the two pinching cases. This is especially noticeable for sensors 2, 3, 7, 10 and 14. As expected, several sensors (2, 3, 7 and 14) placed in the fingertips are more compressed when there is a chopstick in between the

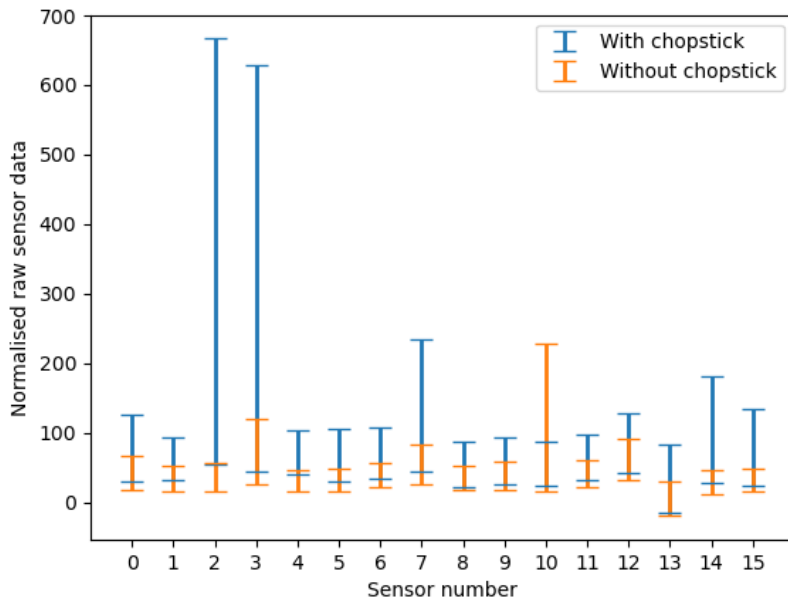


Figure 4.5: Comparison of results between sensor data when pinching with and without chopstick in between index and thumb.

fingertips. This makes sense since the applied displacement by the servomotor is identical so the soft skin deforms considerably more where it is in contact with the chopstick. Sensor number 10's lower reading with a chopstick suggest that the chopstick prevented this chamber from being compressed. It is unlikely for any sensor in the fingertips to be less compressed due to the nature of the soft skin which would deform over an area larger than the size of the chopstick. Sensor 10 is positioned in the interphalangeal (IP) joint of the thumb as shown in Figure 3.7. It is therefore not surprising that its value is lowered as the chopstick prevents this joint from further flexing. This specific example reveals how these types of chambers can be used not only for tactile sensing but also internal deformation and bending in soft bodies. Further work could focus on determining joint angles and states from such sensor data.

These results are very promising for data interpretation. Sensor readings clearly differ in different picking scenarios and each seems to have a specific ‘image’ associated with the shape and relative position of the object. This information can be used in a closed-loop controller to achieve stable picking. By knowing what the sensor signals look like for an ideal grasping state, the position of the hand and fingers can be adjusted to reach that specific state.

Another key point shown by this experiment is the importance of the materials properties used for the hand and skin. This experiment was performed in an open-loop fashion, with no feedback, the control of the servomotor didn't require adjusting throughout the pickings and none of the attempts to pick up the chopstick failed. Such success can be attributed to the embedded compliancy in the skeletal structure which adjusts its position to fit the object shape and remain in a stable grasp. The soft skin also wraps around the thin chopstick and the silicone rubber prevents it from slipping. Small variations in chopstick position and orientation between successive iterations were passively absorbed by the soft properties of the system.

4.2.2 Orientation Prediction with Neural Networks

Chopstick picking has revealed the existence of underlying patterns and information in the sensor data for a basic manipulation task. Such data must now be successfully interpreted so that a control may make use of it. By using the deep learning API Keras (TensorFlow library), neural networks were designed and trained to obtain a mapping from the sensor inputs to robot state. This data-driven method allows to bypass the impractical modelling of the non-linear deformations of the soft skin. Two different types of models were trained to investigate the effect of the time response in sensor data (observed in Figure 4.3 and Figure 4.4) on data interpretation: a classic Artificial Neural Network (ANN) and a Long Short-Term Memory neural network (LSTM). The first simply processes the 16 sensor inputs in a forward direction while the second captures any sequential information

Table 4.3: Summary of neural network topologies, training data, hyperparameters and output results for ANN and LSTM.

Network type	ANN		LSTM	
	Layer	O/P dim.	Layer	O/P dim.
Model summary	Dense	32	LSTM	10
	Dense	8	Dense	3
	Dense	3		
Data points		16384		16384
Training data		75% Shuffled		75% Unshuffled
Training epochs		50		500
Batch size		32		128
Testing MSE		0.446		0.440

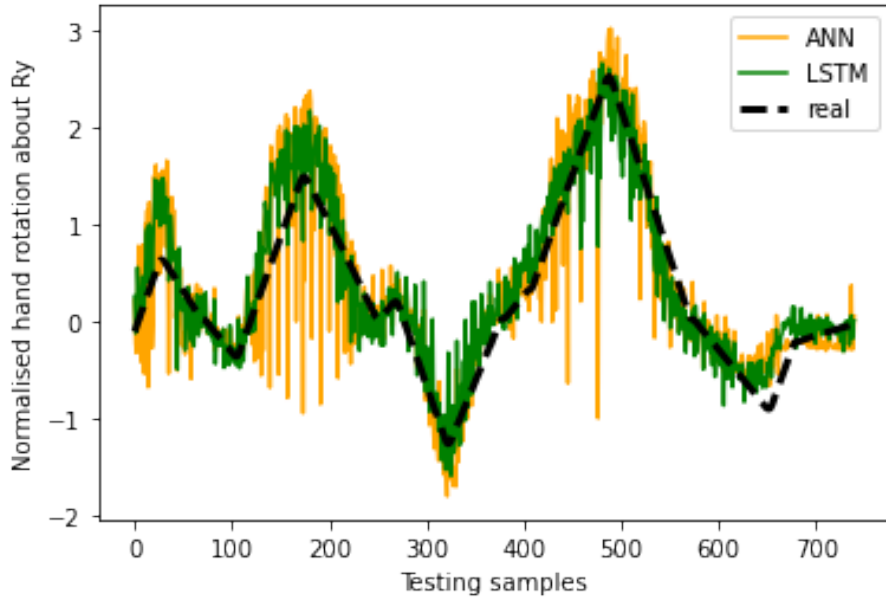


Figure 4.6: Comparison of hand orientations between real data and predictions from the ANN and LSTM neural networks.

from the dataset. Both models were trained with 16384 data points which each include the 16 sensor values (inputs) and 3-axis orientation values (outputs). For both models, the loss function and optimizing algorithm were Mean Squared Error (MSE) and Adam respectively. A summary of each model and results is shown in Table 4.3.

Figure 4.6 shows an example of hand position predictions when providing the trained networks with sensor data from the testing dataset. Dimensionless normalised inputs are used to improve the convergence of the networks when training. As shown by Table 4.3, the mean squared error obtained on the validation data for the LSTM network is only slightly lower than the ANN's. This minor difference is likely due to the fact that the sensors have a rapid response time and provide very repeatable data therefore limiting the possible benefits of taking into sequential information in the LSTM network. Results from both networks nonetheless remain very satisfactory, it is evident that the relative surface orientation between the hand and contact surface can be deduced solely using sensor data once a sufficient amount of interactions have been recorded. As seen in Figure 4.6,

there is still a high level of noise. It can be filtered out as post processing or further experimentation with the neural network topologies may reduce the noise. Although the data is inherently very noisy as shown in a following section, this may be accentuated by an overfitting of the neural networks which may be mitigated by reducing the network sizes.

4.2.3 Hole Detection and Peg-in-hole Problem

Having shown good individual sensor performance and the capability to interpret raw data, the following stage is to use a tool for exploration and remote sensing. As detailed in the previous chapter, to enable a prediction of what size hole is detectable using a tool (chopstick), the minimum change in angle must first be determined. This is similar to sensor characterisation. Figure 4.7 shows sensor data for 4 separate sensors embedded in the the thumb and index. This data has been through a low pass filter to remove unwanted noise and extract the oscillatory behaviour imposed by the UR5 motion. These sensors match the sensors shown in Figure 3.11. As expected from Figure 3.11, signals from sensors 3 and 7 are in phase and 180° out of phase with 14 and 0. By displacing the top of the chopstick an increasing amount (Y displacement on Figure 4.7), the sensor readings show an increasing signal to noise ratio (SNR). When the SNR becomes greater than 1, it becomes possible to reliably detect that there has been a displacement of the chopstick by observing only sensor data. The SNR of 1 corresponds to a displacement of approximately $d = 4\text{mm}$ of the top of the chopstick, therefore a change in angle $\Delta\alpha = \tan^{-1}\left(\frac{d}{L_{chopstick}}\right) = 1.3^\circ$. By substituting this into (3.1), the blue curve is obtained, defining the minimum hole diameter detectable when dragging the chopstick along a flat surface (blue curve of Figure 4.8). As expected, the closer the chopstick to the vertical, the smaller the holes that can be detected.

Having determined the minimum angle detectable and using Equation 3.1 derived previously, experimental data can be collected to verify the model created. Data points were collected by positioning the chopstick at a known angle and dragging it along decreasingly sized holes until undetected, at which point the system recorded its last detected hole as the minimum. Figure 4.8 show this minimum detectable hole size for pre-defined angles α . These corroborate the theoretical prediction with a mean error between prediction and measured diameter of 8.9% .

Overall, this experiment illustrates how simplified modelling is possible and useful in understanding interactions between the skin, tool and the environment. This type of tool-use task can be achieved and predicted thanks to the compliancy of the design and careful sensor placement. This gives an example of how air chamber placement is very important in order to perform specific tasks. This experiment is used as a proof of concept rather than an in depth characterisation of the sensors. However, the errors seen

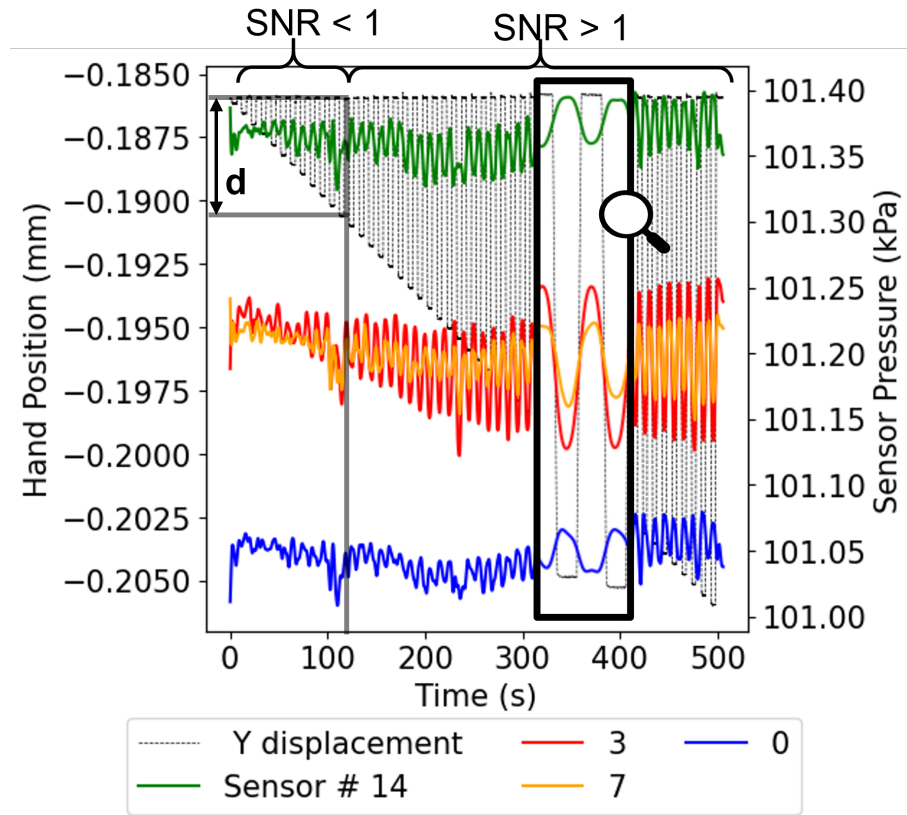


Figure 4.7: Data collection for minimum angle detectable. Minimum detectable displacement $d = 4\text{mm}$ ($\Delta\alpha = 1.3^\circ$).

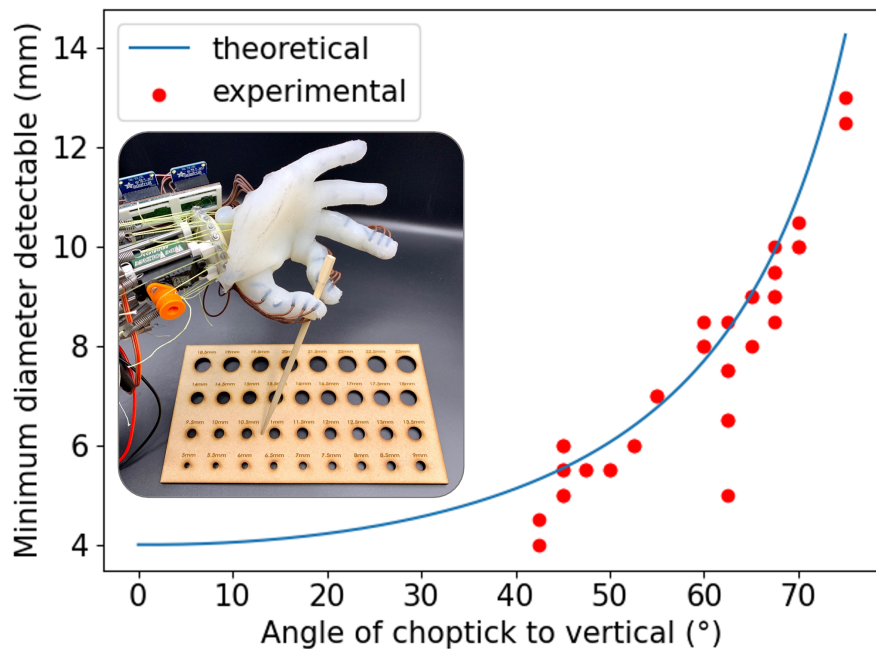


Figure 4.8: Experimental and theoretical (from (3.1)) results showing the smallest hole diameter detected for varying chopstick angle α , with experimental setup shown (left).

in Figure 4.8 are worth discussing. As seen in Figure 4.2, location and distance between the skin contact and air chamber position has a significant effect on sensitivity which in turns affects what change in angle or hole diameter the sensors can reliably detect. This is where data-driven approaches to sensing can improve results, by increasing the training dataset with slightly noisier data, the network's model can account for imprecisions in contact locations.

4.3 Noise analysis

Control often requires signal processing stages of the raw data before attempting data interpretation. The use of a low-pass filter in the previous experiments is part of such signal processing stages. The level of noise can have a big impact on the ability to control a system. Understanding where noise comes from and its behaviour enables us to mitigate the effect of noise sources, implement better signal processing algorithms and achieve more reliable control.

Noise is pervasive in any physical sensory acquisition system, Figure 4.9 shows how noisy the raw signal is. This figure takes data from the Figure 4.7 as a case study for an analysis of the noise present in sensor data. Figure 4.9 shows both the raw sensor signal as well as the filtered signal that was used in the experiment. The filtering is a simple low-pass filter set at 0.2Hz frequency. The oscillation period for the experiment was 10 seconds. Following the Nyquist theorem, to recover the shape of the signal, the

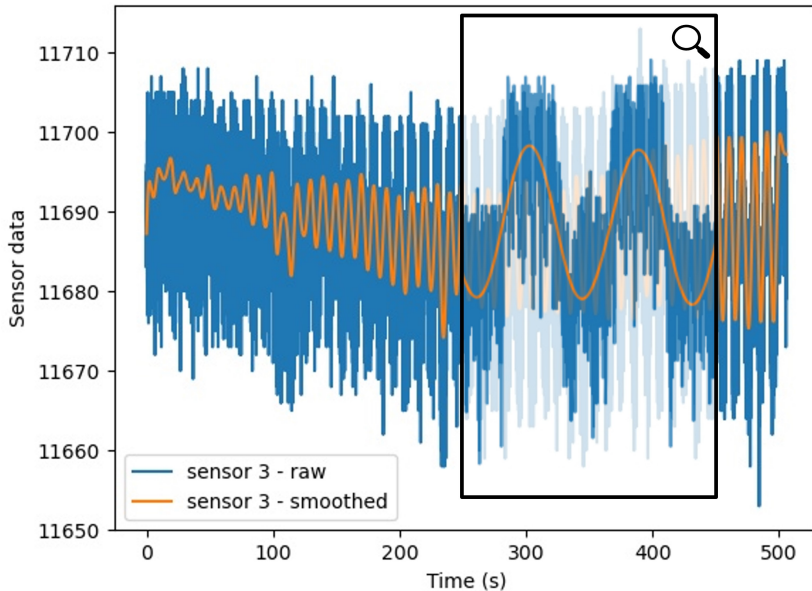


Figure 4.9: Example of raw and smoothed low-pass filtered (0.2Hz) signals for minimum detectable angle, data from Figure 4.7. Raw sensor data is dimensionless.

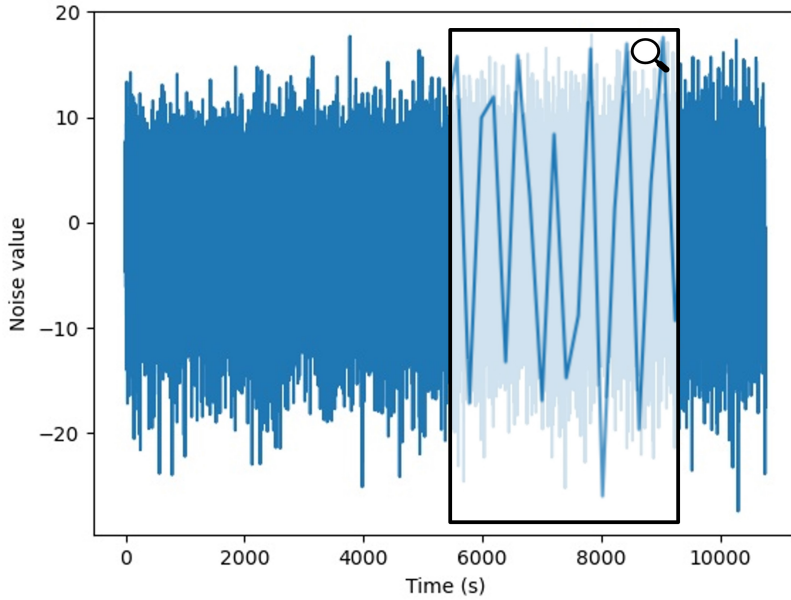


Figure 4.10: High-pass filter (0.2Hz) applied to raw signal of Figure 4.9.

information must be sampled at a frequency greater than or equal to twice per cycle, giving $f = 2 \times 1/T = 2/10 = 0.2\text{Hz}$. Although the input signal isn't perfectly sinusoidal, this is a valid assumption which was shown to have good results in the previous section. This section doesn't consider the smoothed, low-pass filtered signal, but the high-pass filtered signal, which is the sensor noise. The output of a 0.2Hz high-pass filter is shown in Figure 4.10. To analyse this signal, it can be transformed into a histogram. Each bar represents a specific range of values in the signal and its height shows the number of values that are in that range. The histogram of the high-pass noise signal is shown in green in Figure 4.11.

The shape of the histogram can help understand the distribution of the noise. At first glance it appears that the noise sources are split into two empirically determined Gaussian functions, with approximate mean and variance specified in Figure 4.11's legend. The two Gaussian functions are shown in blue, and by summing them before normalising the new probability density for its integral to be equal to 1, the red curve is obtained. This corresponds well to the noise distribution experimentally measured. Although it is by no means an accurate depiction of the noise for all sensors, such technique shows that it is possible to model and understand the sensor noise in the hope of mitigating its sources. Modelling the noise sources also enables the controller to recognise it and take it into account when processing raw data.

Having modelled the noise, it is interesting to question what the potential sources are. As stated in [61]: “When measurement errors are the result of the additive combination of a large number of small underlying errors, the resulting distribution of measurement error

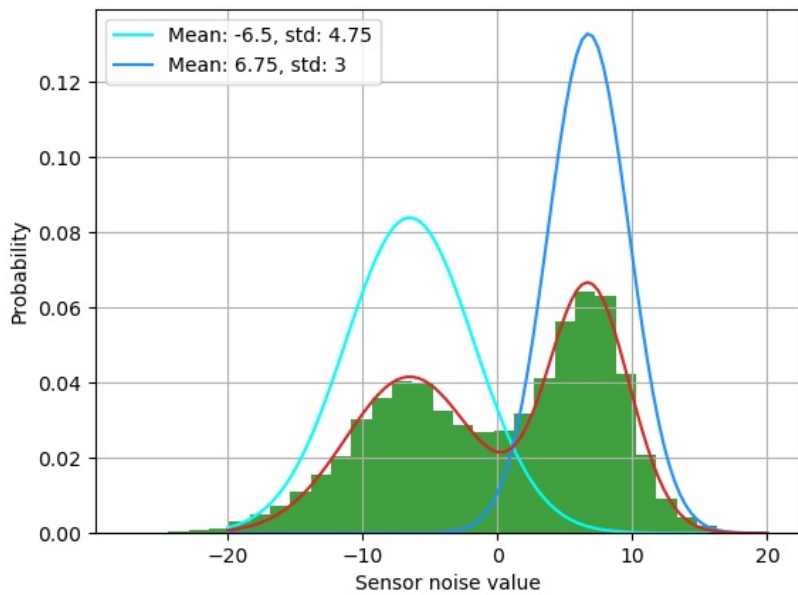


Figure 4.11: Noise analysis using sum of Gaussian functions, noise value probabilities from signal shown in Figure 4.10.

will follow a Gaussian distribution". It is therefore natural for natural noise sources to take a Gaussian shape. There are many possible sources in our system, Table 4.4 provides a non-exhaustive list of such sources and possible solutions.

Table 4.4: Sensor noise sources and mitigating solutions.

Noise type	Source	Possible solution
Electrical	<p>There are many sources of noise in electrical circuits themselves for example including electromagnetic interference (EMI) or crosstalk. The latter is caused by different systems operating in parallel in circuits or channels which are linked together for example through their power source.</p>	<p>To reduce electrical noise, it is possible to increase the operating voltages to improve the signal to noise ratio. However, this is often limited by the components used. This also comes to the cost of raised power dissipation. Isolating the circuits used to drive and control the servomotor and the sensors would likely reduce the amount of noise transmitted to the sensors from the actuator circuitry. Shielding or twisting cables can also help to reduce EMI.</p>
Temperature	<p>The random thermal motion of charge carrier leads to noise in electrical circuits. Moreover, temperature changes can result in different noise. This is typically taken into account in integrated circuits which are often designed to include temperature compensation circuitry. This is shown in the datasheet of the pressure sensor used in this thesis, MPXH6300A [62].</p>	<p>To mitigate this, the circuitry can be cooled down using heatsinks however some level of thermal noise is unavoidable.</p>
Miscellaneous	Any	<p>Filtering stages post data collection don't reduce the generated noise but can nonetheless simplify data interpretation. There are many filtering techniques possible, such as: mean (convolution) filtering, median filtering and Gaussian smoothing.</p>

Chapter 5

Conclusions

5.1 Main Findings

In this thesis, the design and manufacturing process of a soft barometric sensorised skin were detailed to propose a solution for improving robotic manipulation capabilities. The sensing skin does not come with the cost of interfering with the passive dynamics of the soft components. By applying the skin to an existing anthropomorphic robotic hand, all functions required for tool use can be successfully achieved. This includes picking, data interpretation for exploration and in-hand manipulation as well as exteroception. With careful arrangement of sensing receptors around fingertips, multiple applications can be considered including: surface orientation detection for in-hand manipulation; and hole detection through a grasped object for feedback during tool-use.

The barometric soft sensing skin demonstrates good performance and receptor density, with a sensitivity range from $0.023V/N$ to $0.11V/N$, time response $<50ms$ and repeatability of sensor response aside from resting air pressure drift. This is shown by a series of characterising experiments on a sample skin. The configurable design allows to control sensitivity to different tactile stimuli (pressure, area, location). This has potential to detect other stimuli such as skin stretch or joint bending, giving excellent versatility and multi-modal sensing with a single manufacturing process.

Finally, the selected design and materials enable fast prototyping and manufacturing stages. This approach to a soft sensorised skin is highly configurable; the air chambers and pressure sensors can be easily placed in any location of the skin. Moreover, the nature of this implementation allows for easy customisation to any morphology of anthropomorphic hand or gripper with little design constraints. This solution is low-cost compared to many technologies, relying on off-the-shelf electronic components and sensors as well as readily available materials for 3D printing and casting.

5.2 Limitations

There are several limitation which were revealed throughout the work. This section includes a discussion of such limitations and possible solutions.

- The lack of modelling and simulation environment for such an application of soft robotics makes it difficult to analytically establish an optimal solution when it comes to material selection, air chamber locations and air chamber shapes in the skin. From the literature it appears that even if using specialized finite element analysis (FEA) software, it would be complex to simulate the details of the design which includes both a compliant skeletal structure and soft skin. Sim-to-real transferability is also raised as one of the bottlenecks when it comes to simulations.
- For these reasons, a model-free, data-driven approach was selected for data interpretation in this project. This issue with this is that it is often task specific. Transferability between tasks is possible to some extent [54], but limited to tasks with similar sensor readings. Therefore, data must be collected and processed for each possible task, requiring ample time and computer resources. However, this is arguably the approach humans use as they grow up and learn how to interact with their surroundings, suggesting that it may be a viable solution.
- In this project, one of the limitations was the data rate when sampling from a large array of sensors. The theoretical limit of the analog-digital converters is 860Hz while just above 60Hz were achieved using the presented framework. By improving the sampling rate of sensors, tasks involving rapid controllers perform better, for example if attempting surface or contour following in tactile servoing applications.
- When it comes to the density of sensors, it was limited by the relatively bulky electronics and tubing which were placed on the back of the hand. Improving the design and their integration could allow for a higher air chamber density in the skin and as a result more accurate sensing. As shown by many biological systems, having an increased number of sensors improves the success rate of feedback-based tasks as long as the data can be processed in time.
- The dexterity of the hand itself was also a limiting factor to perform dexterous tasks that could fully exhibit the sensing skin's potential. A single actuator to perform pinching is the bare minimum to enable active manipulation. An increased number of actuators complexifies the controller implementation but enables increased dexterity.

5.3 Future work

The technologies and framework presented have shown the potential of a soft sensing skin for improved robotic manipulation. To extend this work and further this research, a number of directions are proposed.

Work should be done on the current system to improve its performance enabling better results for the tasks presented and enabling further more complex manipulation problems. Finding the bottleneck in sensor sampling rate and upgrading the electronic components used is a first step which would contribute to this. Mitigating the sensor noise, by exploring noise sources through experiments and replacing breadboards with custom designed PCBs would further help improve the current implementation.

Refactoring the design and CAD by embedding air channels in the manufacturing steps (e.g. EMB3D printing [63]) would enable an increased sensor density. This could include replacing the externally routed flexible tubing with soft channels embedded in the skin, routing through the skeletal structure or bring the pressure sensors closer to the air chambers. Sensors could be embedded in the 3D printed bones without impacting the soft properties of the skin. This approach would also reduce the clutter from all the flexible tubing and electronics currently attached to the wrist of the hand.

Currently, the sensor air chambers have only been used to detect and measure normal forces and deformations of the skin. By experimenting with different air chamber shapes, notably asymmetrical shapes (e.g. parallelograms), it appears that such chambers have directional responses to shearing forces and skin deformation. Further investigation should be done to see if an array of such chambers can produce a resultant vector to indicate the direction and magnitude of shearing motion. If such sensor is able to detect both normal and tangential forces, the grasping stability could be considerably improved, especially for tasks involving possible slip of objects. This would be a fully soft implementation of a 3-DOF sensor.

This novel approach to soft tactile sensing opens many directions for research that could enable modern robots to better manipulate objects, increase the diversity of possible tasks and as a consequence improve their integration in human environments.

Bibliography

- [1] C Piazza et al. “A century of robotic hands”. In: *Annual Review of Control, Robotics, and Autonomous Systems* 2 (2019), pp. 1–32.
- [2] Antonio Bicchi. “Hands for dexterous manipulation and robust grasping: A difficult road toward simplicity”. In: *IEEE Transactions on robotics and automation* 16.6 (2000), pp. 652–662.
- [3] JAE Hughes, P Maiolino, and Fumiya Iida. “An anthropomorphic soft skeleton hand exploiting conditional models for piano playing”. In: *Science Robotics* 3.25 (2018).
- [4] Gionata Salvietti. “Replicating human hand synergies onto robotic hands: A review on software and hardware strategies”. In: *Frontiers in neurorobotics* 12 (2018), p. 27.
- [5] Jianshu Zhou et al. “A soft-robotic approach to anthropomorphic robotic hand dexterity”. In: *IEEE Access* 7 (2019), pp. 101483–101495.
- [6] Clemens Eppner et al. “Exploitation of environmental constraints in human and robotic grasping”. In: *The International Journal of Robotics Research* 34.7 (2015), pp. 1021–1038.
- [7] Ravinder Dahiya et al. “Large-area soft e-skin: The challenges beyond sensor designs”. In: *Proceedings of the IEEE* 107.10 (2019), pp. 2016–2033.
- [8] Yuneng Tang et al. “Recent Advances of 4D Printing Technologies Toward Soft Tactile Sensors”. In: *Frontiers in Materials* 8 (2021). ISSN: 2296-8016. DOI: 10.3389/fmats.2021.658046. URL: <https://www.frontiersin.org/article/10.3389/fmats.2021.658046>.
- [9] Zhanat Kappassov, Juan Antonio Corrales Ramon, and Veronique Perdereau. “Tactile sensing in dexterous robot hands — Review”. In: *Robotics and Autonomous Systems* 74 (July 2015). DOI: 10.1016/j.robot.2015.07.015.
- [10] M. Zhang and A. F. T. Mak. “In vivo friction properties of human skin”. In: *Prosthetics and Orthotics International* 23.2 (1999). PMID: 10493141, pp. 135–141. DOI: 10.3109/03093649909071625. eprint: <https://doi.org/10.3109/03093649909071625>. URL: <https://doi.org/10.3109/03093649909071625>.
- [11] Zhe Xu and Emanuel Todorov. “Design of a highly biomimetic anthropomorphic robotic hand towards artificial limb regeneration”. In: May 2016, pp. 3485–3492. DOI: 10.1109/ICRA.2016.7487528.
- [12] Ashish Deshpande et al. “Anatomically correct testbed hand control: Muscle and joint control strategies”. In: May 2009, pp. 4416–4422. DOI: 10.1109/ROBOT.2009.5152542.
- [13] Zhe Xu, Svetoslav Kolev, and Emanuel Todorov. “Design, optimization, calibration, and a case study of a 3D-printed, low-cost fingertip sensor for robotic manipulation”. In: *2014 IEEE International Conference on Robotics and Automation (ICRA)*. 2014, pp. 2749–2756. DOI: 10.1109/ICRA.2014.6907253.
- [14] Naoki Fukaya et al. “Development of a five-finger dexterous hand without feedback control: The TUAT/Karlsruhe humanoid hand”. In: Nov. 2013, pp. 4533–4540. DOI: 10.1109/IROS.2013.6697008.
- [15] Akihiko Yamaguchi and Christopher G Atkeson. “Recent progress in tactile sensing and sensors for robotic manipulation: can we turn tactile sensing into vision?” In: *Advanced Robotics* 33.14 (2019), pp. 661–673.
- [16] Oliver Kroemer, Christoph H. Lampert, and Jan Peters. “Learning Dynamic Tactile Sensing With Robust Vision-Based Training”. In: *IEEE Transactions on Robotics* 27.3 (2011), pp. 545–557. DOI: 10.1109/TRO.2011.2121130.
- [17] Hanna Yousef, Mehdi Boukallel, and Kaspar Althoefer. “Tactile sensing for dexterous in-hand manipulation in robotics—A review”. In: *Sensors and Actuators A: physical* 167.2 (2011), pp. 171–187.
- [18] Benjamin Ward-Cherrier et al. “The tactip family: Soft optical tactile sensors with 3d-printed biomimetic morphologies”. In: *Soft robotics* 5.2 (2018), pp. 216–227.

- [19] Nathan F Lepora et al. “Towards integrated tactile sensorimotor control in anthropomorphic soft robotic hands”. In: *2021 IEEE International Conference on Robotics and Automation (ICRA)*. IEEE. 2021, pp. 1622–1628.
- [20] Gereon H. Büscher et al. “Flexible and stretchable fabric-based tactile sensor”. In: *Robotics and Autonomous Systems* 63 (2015). Advances in Tactile Sensing and Touch-based Human Robot Interaction, pp. 244–252. ISSN: 0921-8890. DOI: <https://doi.org/10.1016/j.robot.2014.09.007>. URL: <https://www.sciencedirect.com/science/article/pii/S0921889014001821>.
- [21] Carlos A. Jara et al. “Control Framework for Dexterous Manipulation Using Dynamic Visual Servoing and Tactile Sensors’ Feedback”. In: *Sensors* 14.1 (2014), pp. 1787–1804. ISSN: 1424-8220. DOI: 10.3390/s140101787. URL: <https://www.mdpi.com/1424-8220/14/1/1787>.
- [22] Panagiotis Polygerinos et al. “Soft robotics: Review of fluid-driven intrinsically soft devices; manufacturing, sensing, control, and applications in human-robot interaction”. In: *Advanced Engineering Materials* 19.12 (2017), p. 1700016.
- [23] Thomas George Thuruthel, Kieran Gilday, and Fumiya Iida. “Drift-Free Latent Space Representation for Soft Strain Sensors”. In: *2020 3rd IEEE International Conference on Soft Robotics (RoboSoft)*. IEEE. 2020, pp. 138–143.
- [24] Vincent Wall, Gabriel Zöller, and Oliver Brock. “A method for sensorizing soft actuators and its application to the RBO hand 2”. In: *2017 IEEE International Conference on Robotics and Automation (ICRA)*. IEEE. 2017, pp. 4965–4970.
- [25] Jessica Yin, Tess Hellebrekers, and Carmel Majidi. “Closing the Loop with Liquid-Metal Sensing Skin for Autonomous Soft Robot Gripping”. In: *2020 3rd IEEE International Conference on Soft Robotics (RoboSoft)*. IEEE. 2020, pp. 661–667.
- [26] Siheng Li et al. “Polyelectrolyte complex-based self-healing, fatigue-resistant and anti-freezing hydrogels as highly sensitive ionic skins”. In: *Journal of Materials Chemistry A* 8.7 (2020), pp. 3667–3675.
- [27] Gabriel Zöller, Vincent Wall, and Oliver Brock. “Acoustic sensing for soft pneumatic actuators”. In: *2018 IEEE/RSJ International Conference on Intelligent Robots and Systems (IROS)*. IEEE. 2018, pp. 6986–6991.
- [28] Yaroslav Tenzer, Leif P. Jentoft, and Robert D. Howe. “The Feel of MEMS Barometers: Inexpensive and Easily Customized Tactile Array Sensors”. In: *IEEE Robotics Automation Magazine* 21.3 (2014), pp. 89–95. DOI: 10.1109/MRA.2014.2310152.
- [29] Lorenzo Jamone et al. “Highly Sensitive Soft Tactile Sensors for an Anthropomorphic Robotic Hand”. In: *IEEE Sensors Journal* 15.8 (2015), pp. 4226–4233. DOI: 10.1109/JSEN.2015.2417759.
- [30] Maria Chiara Carrozza et al. “Design of a cybernetic hand for perception and action”. In: *Biological Cybernetics* 95 (2006), pp. 629–644.
- [31] Loeb G.E Wettels N. Fishel J.A. “Multimodal Tactile Sensor. In: Balasubramanian R., Santos V. (eds) The Human Hand as an Inspiration for Robot Hand Development”. In: *Springer Tracts in Advanced Robotics* 95 (2014), pp. 405–429. DOI: https://doi.org/10.1007/978-3-319-03017-3_19.
- [32] Yashraj S. Narang et al. “Interpreting and predicting tactile signals for the SynTouch BioTac”. In: *The International Journal of Robotics Research* 40.12-14 (2021), pp. 1467–1487. DOI: 10.1177/02783649211047634. eprint: <https://doi.org/10.1177/02783649211047634>. URL: <https://doi.org/10.1177/02783649211047634>.
- [33] Thomas George Thuruthel et al. “Using Redundant and Disjoint Time-Variant Soft Robotic Sensors for Accurate Static State Estimation”. In: *IEEE Robotics and Automation Letters* 6.2 (2021), pp. 2099–2105.
- [34] Juan Antonio Corrales Ramón, Véronique Perdereau, and Fernando Torres Medina. “Multi-fingered robotic hand planner for object reconfiguration through a rolling contact evolution model”. In: *2013 IEEE International Conference on Robotics and Automation*. 2013, pp. 625–630. DOI: 10.1109/ICRA.2013.6630638.
- [35] Maria Teresa Francomano, Dino Accoto, and Eugenio Guglielmelli. “Artificial Sense of Slip—A Review”. In: *IEEE Sensors Journal* 13.7 (2013), pp. 2489–2498. DOI: 10.1109/JSEN.2013.2252890.
- [36] Georg Stillfried et al. “MRI-Based Skeletal Hand Movement Model”. In: *The Human Hand as an Inspiration for Robot Hand Development*. Ed. by Ravi Balasubramanian and Veronica J. Santos. Cham: Springer International Publishing, 2014, pp. 49–75. ISBN: 978-3-319-03017-3. DOI: 10.1007/978-3-319-03017-3_3. URL: https://doi.org/10.1007/978-3-319-03017-3_3.
- [37] Ravinder S. Dahiya et al. “Directions Toward Effective Utilization of Tactile Skin: A Review”. In: *IEEE Sensors Journal* 13.11 (2013), pp. 4121–4138. DOI: 10.1109/JSEN.2013.2279056.
- [38] Lael U. Odhner et al. “A compliant, underactuated hand for robust manipulation”. In: *The International Journal of Robotics Research* 33.5 (2014), pp. 736–752. DOI: 10.1177/0278364913514466. eprint: <https://doi.org/10.1177/0278364913514466>. URL: <https://doi.org/10.1177/0278364913514466>.

- [39] Ellen Roels et al. “A Multi-Material Self-Healing Soft Gripper”. In: *2019 2nd IEEE International Conference on Soft Robotics (RoboSoft)*. 2019, pp. 316–321. DOI: [10.1109/ROBOSOFT.2019.8722781](https://doi.org/10.1109/ROBOSOFT.2019.8722781).
- [40] Risto Kõiva et al. “A highly sensitive 3D-shaped tactile sensor”. In: *2013 IEEE/ASME International Conference on Advanced Intelligent Mechatronics*. 2013, pp. 1084–1089. DOI: [10.1109/AIM.2013.6584238](https://doi.org/10.1109/AIM.2013.6584238).
- [41] Qiang li et al. “A Control Framework for Tactile Servoing”. In: June 2013. DOI: [10.15607/RSS.2013.IX.045](https://doi.org/10.15607/RSS.2013.IX.045).
- [42] Kieran Gilday, Thomas George Thuruthel, and Fumiya Iida. “A Vision-Based Collocated Actuation-Sensing Scheme for a Compliant Tendon-Driven Robotic Hand”. In: May 2020, pp. 760–765. DOI: [10.1109/RoboSoft48309.2020.9116054](https://doi.org/10.1109/RoboSoft48309.2020.9116054).
- [43] Philip Moseley et al. “Modeling, design, and development of soft pneumatic actuators with finite element method”. In: *Advanced Engineering Materials* 18.6 (Dec. 2015), pp. 978–988. DOI: [10.1002/adem.201500503](https://doi.org/10.1002/adem.201500503).
- [44] Sam Kriegman et al. “Scalable sim-to-real transfer of soft robot designs”. In: *2020 3rd IEEE International Conference on Soft Robotics (RoboSoft)*. 2020, pp. 359–366. DOI: [10.1109/RoboSoft48309.2020.9116004](https://doi.org/10.1109/RoboSoft48309.2020.9116004).
- [45] Toby Howison et al. “Reality-assisted evolution of soft robots through large-scale physical experimentation: a review”. In: *CoRR* abs/2009.13960 (2020). arXiv: 2009.13960. URL: <https://arxiv.org/abs/2009.13960>.
- [46] Robert Kwiatkowski and Hod Lipson. “Task-agnostic self-modeling machines”. In: *Science Robotics* 4 (Jan. 2019), eaau9354. DOI: [10.1126/scirobotics.aau9354](https://doi.org/10.1126/scirobotics.aau9354).
- [47] Seunghyun Han et al. “Use of Deep Learning for Characterization of Microfluidic Soft Sensors”. In: *IEEE Robotics and Automation Letters* 3.2 (2018), pp. 873–880. DOI: [10.1109/LRA.2018.2792684](https://doi.org/10.1109/LRA.2018.2792684).
- [48] Xiaofeng Yuan, Lin Li, and Yalin Wang. “Nonlinear Dynamic Soft Sensor Modeling With Supervised Long Short-Term Memory Network”. In: *IEEE Transactions on Industrial Informatics* 16.5 (2020), pp. 3168–3176. DOI: [10.1109/TII.2019.2902129](https://doi.org/10.1109/TII.2019.2902129).
- [49] Herke Hoof et al. “Learning robot in-hand manipulation with tactile features”. In: Nov. 2015, pp. 121–127. DOI: [10.1109/HUMANOIDS.2015.7363524](https://doi.org/10.1109/HUMANOIDS.2015.7363524).
- [50] Nathan Lepora and John Lloyd. “Pose-based tactile servoing: Controlled soft touch using deep learning”. In: *IEEE Robotics & Automation Magazine* (2021).
- [51] Stephen Tian et al. “Manipulation by Feel: Touch-Based Control with Deep Predictive Models”. In: *CoRR* abs/1903.04128 (2019). arXiv: 1903.04128. URL: <http://arxiv.org/abs/1903.04128>.
- [52] Giada Gerboni et al. “Feedback control of soft robot actuators via commercial flex bend sensors”. In: *IEEE/ASME Transactions on Mechatronics* 22.4 (2017), pp. 1881–1888.
- [53] Wenzhen Yuan, Siyuan Dong, and Edward H. Adelson. “GelSight: High-Resolution Robot Tactile Sensors for Estimating Geometry and Force”. In: *Sensors* 17.12 (2017). ISSN: 1424-8220. DOI: [10.3390/s17122762](https://doi.org/10.3390/s17122762). URL: <https://www.mdpi.com/1424-8220/17/12/2762>.
- [54] Kieran Gilday, Josie Hughes, and Fumiya Iida. “Wrist-driven passive grasping: interaction-based trajectory adaption with a compliant anthropomorphic hand”. In: *Bioinspiration & Biomimetics* 16.2 (2021), p. 026024.
- [55] Lukas Kaul et al. “The sense of surface orientation — A new sensor modality for humanoid robots”. In: *2016 IEEE-RAS 16th International Conference on Humanoid Robots (Humanoids)*. 2016, pp. 820–825. DOI: [10.1109/HUMANOIDS.2016.7803368](https://doi.org/10.1109/HUMANOIDS.2016.7803368).
- [56] Kurt Hornik, Maxwell Stinchcombe, and Halbert White. “Multilayer feedforward networks are universal approximators”. In: *Neural Networks* 2.5 (1989), pp. 359–366. ISSN: 0893-6080. DOI: [https://doi.org/10.1016/0893-6080\(89\)90020-8](https://doi.org/10.1016/0893-6080(89)90020-8). URL: <https://www.sciencedirect.com/science/article/pii/0893608089900208>.
- [57] *Linear Solenoids*. Dec. 2021. URL: <https://www.geeplus.com/linear-solenoids-2/>.
- [58] Inc. Interlink Electronics. *FSR sensor, force sensing resistor*. URL: <https://www.interlinkelectronics.com/force-sensing-resistor>.
- [59] *Pressure measurement and mapping sensors*. URL: <https://pressureprofile.com/sensor-systems/sensors>.
- [60] Hanafiah Yussof et al. “Tactile Sensing-based Control System for Dexterous Robot Manipulation”. In: *Advances in Computational Algorithms and Data Analysis*. Ed. by Sio-Iong Ao, Burghard Rieger, and Su-Shing Chen. Dordrecht: Springer Netherlands, 2009, pp. 199–213. ISBN: 978-1-4020-8919-0. DOI: [10.1007/978-1-4020-8919-0_15](https://doi.org/10.1007/978-1-4020-8919-0_15). URL: https://doi.org/10.1007/978-1-4020-8919-0_15.
- [61] Phillip Stanley-Marbell. *Foundations of embedded systems, topic 02: Uncertainty*. 2019. URL: <https://f-of-e.org/chapter-02>.

- [62] *MPXH6300A, 20 to 300 KPA, absolute, integrated, pressure sensor - NXP*. Sept. 2015. URL: <https://www.nxp.com/docs/en/data-sheet/MPXH6300A.pdf>.
- [63] Michael Wehner et al. “An integrated design and fabrication strategy for entirely soft, autonomous robots”. In: *nature* 536.7617 (2016), pp. 451–455.

Website citations were all accessed on the 1st of June 2022

Chapter 6

Appendices

Risk Assessment Retrospective

A risk assessment form was submitted at the start of this project to identify and mitigate potential hazards. Following is a short review of the hazards identified, there were no accidents during the project.

- Manufacturing related hazards including the use of workshop tools, soldering or working with toxic materials (e.g. resins for castings). These risks were well understood and carefully mitigated by taking appropriate safety measures including wearing PPE and keeping areas well ventilated.
- Risk relating to the use of powerful robots (i.e. UR5) were successfully avoided by always having the emergency stop button at close proximity and remaining a certain distance away when trying new code. Early on, it was revealed that the robotic arm moving directly to its home position when connecting to it could involve uncontrolled large and rapid motion. This was especially a risk when changing task, moving the robot manually to another position or coming back to experiment with the robot after a few days. To mitigate the risk of forgetting to update the home position properly, a rapid user confirmation was implemented in the software, allowing to set the current position as the new home when connecting to the robot.
- The amount of work required next to the robotic arms was underestimated when writing the initial risk assessment, a better desk and chair setup could have been used to improve comfort. This should be tackled as early as possible in the project.
- Finally, keeping a tidy and clean workspace and lab environment also helps reduce the number of hazards and potential damage to equipment used.

Acknowledgements

This project was co-supervised and completed with contributions from Kieran Gilday, a PhD student in the Bio-Inspired Robotics Lab, supervised by Dr F. Iida.

A research paper was also submitted to the IROS conference from the research done for this project:

Kieran Gilday, Louis Relandreau, Fumiya Iida, "*Design and Characterisation of a Soft Barometric Sensing Skin for Robotic Manipulation*", IROS 2022.

Additional Resources

A logbook was submitted alongside this thesis, uploaded via Moodle to show the workflow throughout the year.

A GitHub repo containing the source code for all software implementation and data is provided at the following link: <https://github.com/louis-relandreau/IIB-Project-Soft-Sensing>. Below is a copy of the README.md documentation for this repo.

IIB Project: Precise tool manipulation and positioning of a soft sensorised anthropomorphic hand through feedback control and machine learning

This documentation is provided as a complement to the Master's thesis submitted. It contains a description of the main software used in this project. The software and relevant data has been uploaded to the following [repo](#) which contains a formatted duplicate of this README.

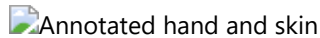


Image showing the novel soft sensing (pressure sensors) skin mounted onto an anthropomorphic robotic hand.

<https://user-images.githubusercontent.com/50178739/171024593-bebd515f-bac5-401d-b536-4ae33388a96d.mp4>

Video illustrating examples of picking and in real time sensing using tools.

Table of contents:

- Main controllers: This folder includes all of the software used to control the UR5 robotic arm, the hand servomotor and the read the sensors' data. It also includes the data from all the performed experiments as well as any code used for signal processing or visualising the results.
- Neural networks: This folder contains the code implementations and results of the neural networks used for data interpretation of the surface orientation prediction experiment.
- CAD: This includes the CAD models generated for any part that required 3D printing or casting during the various experiments. The CAD of the hand and skin itself isn't included, its Kieran Gilday proprietary resources.
- Media: A few images and videos of the robots, experimental setups and results to showcase the project's system.

Main controller

This section describes the controller used for experiments and data collection in this project. It is based off previous work done in the Bio-Inspired Robotics Lab ([BIRL](#)), notably PhD student Kieran Gilday. This [GitHub repo](#) contains the generic code that was used a base for the UR5 controller and client software. For details on how the connection with the UR5 is setup, how to load the program on the robot and setup IP ports adequately, please refer to the aforementioned [GitHub repo](#).

Contents

The Main-controller folder contains [ur5_and_hand_controller](#) which is the directory containing all controllers, collected data and function used for plotting. The data, the plotting functions as well as the functions used to collect said data are all named appropriately and briefly commented on in the code.

It also contains [Arduino](#), which is all the code used for sensor polling and servomotor control. This code should be uploaded to an Arduino or equivalent following the indicated pin numbering to allow for a

controller to communicate with it.

This folder also contains [ur5_client](#), the code used on the UR5 client which is required to interface with the python script. This should be loaded on the UR5 system previously to any connection, see below.

Libraries in use:

- numpy
- matplotlib
- csv
- cv2
- json
- math
- time
- scipy
- random
- pathlib
- _thread
- socket

Getting Started:

- Main loop in [Generic_ur5_controller.py](#), contains examples of using kg_robot and teach mode. The modified implementation used in the thesis is presented in [sensing_hand.py](#).
- The robot is controlled using the functions defined in [kg_robot.py](#) in the ur5 commands section, if the desired robot function doesn't exist and cannot be created through a combination of existing functions, it can be added by modifying kg_robot.py and kg_client.urp. Complete capabilities are described in [ur5 script api](#).
- Specialized robot functions and complex sequences which include robot motion, cameras, hand actuation, data recording are called from [sensing_hand.py](#) and defined in [skin_sense.py](#)
- [Waypoints.py](#) is used for global robot poses, joints and tool centre points (tcp) which can be called by any function.
- To improve safety and ensure that the robot doesn't move rapidly to a previously defined position that may now be obstructed, a check is implemented at the start of [sensing_hand.py](#), as soon as the connection with the UR5 is completed, to assert the location of the new home position and redefine it as the current position if required.

Neural Networks

This section relies on a set of iPython notebook based on a tutorial from [machinelearningmastery](#). The [Neural-networks](#) contains the code used for orientation predictions using an ANN and LSTM network, the data used to train and test these networks, and the obtained results. Folders containing results for each of these implementations are labelled appropriately.

Contents

The folders [orientation_prediction_ANN](#) and [orientation_prediction_LSTM](#) each contain a .iynb file which describe the entire training process and results for each network type. The folders also include the data used for training and testing as well as some images showing training loss and network outputs.

A comparison of both results is included in [ANN-LSTM-comparison.ipynb](#)

Graphs showing results from varying networks and training parameters are included in [media-results](#).

An experiment was attempted to predict the 2D orientation of a pinched chopstick with the bottom end of the chopstick stuck in a fixed ball joint using a similar neural network data-driven approach. Results were inconclusive and disregarded in the thesis but data and training methods are included in [ball_joint](#)

Libraries in use:

- Sklearn
- Keras
- TensorFlow
- Numpy
- Pandas
- Matplotlib
- Csv

Getting Started:

The implementations follow the following structure:

1. Importing the data from a .csv file
2. Processing the raw data to extract suitable dataset and format it appropriately for use in neural networks
3. Splitting the data in training and testing datasets with shuffle if required
4. Define model topology
5. Perform training and plot loss in real time
6. Print an example of prediction from the testing dataset

These steps can be followed to understand the methods used and replicate these techniques for similar problems.